Merve Gül TURAN

A Master's Thesis

AGU 2023

BBSOME REGULATES ARL13B-DEPENDENT JOINT ELONGATION OF TWO DISTINCT CILIA IN *CAENORHABDITIS ELEGANS*

A THESIS
SUBMITTED TO THE DEPARTMENT OF BIOENGINEERING
AND THE GRADUATE SCHOOL OF ENGINEERING AND SCIENCE
OF ABDULLAH GUL UNIVERSITY
IN PARTIAL FULFILLMENT OF THE REQUIREMENTS
FOR THE DEGREE OF
MASTER

By
Merve Gül TURAN
June 2023

BBSOME REGULATES ARL13B-DEPENDENT JOINT ELONGATION OF TWO DISTINCT CILIA IN *CAENORHABDITIS ELEGANS*

A THESIS
SUBMITTED TO THE DEPARTMENT OF BIOENGINEERING
AND THE GRADUATE SCHOOL OF ENGINEERING AND SCIENCE
OF ABDULLAH GUL UNIVERSITY
IN PARTIAL FULFILLMENT OF THE REQUIREMENTS
FOR THE DEGREE OF
MASTER OF SCIENCE

By
Merve Gül TURAN
June 2023

SCIENTIFIC ETHICS COMPLIANCE

I hereby declare that all information in this document has been obtained in accordance with academic rules and ethical conduct. I also declare that, as required by these rules and conduct, I have fully cited and referenced all materials and results that are not original to this work.

Name-Surname: Merve Gül TURAN

Signature :

REGULATORY COMPLIANCE

M.Sc. thesis titled "BBSome regulates ARL13B-dependent joint elongation of two distinct cilia in *Caenorhabditis elegans"* has been prepared in accordance with the Thesis Writing Guidelines of the Abdullah Gül University, Graduate School of Engineering & Science.

Prepared By
Merve Gül TURAN
Signature

Advisor
Asst. Prof. Sebiha CEVİK KAPLAN
Signature

Head of the Bioengineering Program
Asst. Prof. Altan ERCAN
Signature

ACCEPTANCE AND APPROVAL

M.Sc. thesis titled "BBSome regulates ARL13B-dependent joint elongation of two distinct cilia in *Caenorhabditis elegans"* and prepared by Merve Gul Turan has been accepted by the jury in the Bioengineering Graduate Program at Abdullah Gül University, Graduate School of Engineering & Science.

05/06/2023

(Thesis Defense Exam Date)

JURY:

Advisor :Asst. Prof. Sebiha CEVİK KAPLAN

Member :Asst. Prof. Emel Başak GENCER AKÇOK

Member :Prof. Dr. Arzu ÇELIK

APPROVAL:

The acceptance of this M.Sc. thesis has been approved by the decision of the Abdullah Gül University, Graduate School of Engineering & Science, Executive Board dated ….. /….. / …….. and numbered ……..……. .

…….. /…….. / ……..

(Date)

Graduate School Dean
Prof. Dr. İrfan ALAN

ABSTRACT

BBSOME REGULATES ARL13B-DEPENDENT JOINT ELONGATION OF TWO DISTINCT CILIA IN *CAENORHABDITIS ELEGANS*

Merve Gül TURAN

MSc. in Bioengineering

Advisor: Asst. Prof. Sebiha CEVİK KAPLAN

June 2023

Cilia or flagella are interchangeably used to refer to the hair-like organelles extending from the cell surface to communicate with environmental signals or triggers. Cilium, the singular form of cilia, and its components are well-conserved structures throughout evolution and are divided into motile and primary cilium. The primary cilia of different cells are seen to form joint cilia by extending in parallel. For instance, PHA and PHB primary cilia in *C. elegans* protrude from the ends of the dendrite but extend parallel to one another and intersect in the middle portion of the cilia, reaching the same length. Nevertheless, the molecular mechanisms underlying how parallel cilia get similar lengths remain mysterious. In this thesis, we used *C. elagans* as a model organism to examine the molecular mechanism associated with the cilia direction. We generated various single, double, and triple mutants to examine PHA and PHB cilia for phenotype and length. We found that a Joubert syndrome protein, ARL13B, is required for determining cilia direction in PHA & PHB cilia and ASE & ASI cilia.

Keywords: Cilia, BBS, PHA/PHB cilia, cilia-cilia

ÖZET

BBSOME, *CAENORHABDITIS ELEGANS*'TA ARL13B'YE BAĞIMLI İKİ FARKLI SİLYANIN BİRLİKTE UZAMASINI DÜZENLER

Merve Gül TURAN

Biyomühendislik Anabilim Dalı Yüksek Lisans

Tez Yöneticisi: Dr.Öğr.Üyesi Sebiha CEVİK KAPLAN

Haziran 2023

Birbirlerinin yerlerine kullanılan silya ya da flagella, çevresel sinyallerle ve uyaranlarla iletişime giren ve hücre yüzeyinden dış ortama uzanan saç benzeri organellerdir. Tekli silya yapısını ifade eden silyum, and onun alt bileşenleri evrimsel olarak korunmuş yapılarıdır, ve iki gruba ayrılır: hareketli ve birincil. Farklı hücrelerden köken alan birincil silyalar, paralel olarak uzayarak bir noktada birleşir. Örneğin, *C. elegans*'ta bulunan PHA ve PHB silyalar dendritin uçlarından çıkıntı yaparak birbirlerine paralel olarak uzarlar ve orta kısımlarında kesişerek aynı uzunluğa gelirler. Ancak silyaların paralel uzayarak benzer uzunluğa gelmesinin altında yatan moleküler mekanizma bilinmemektedir. Bu tezde, silya yönü ile ilişkili moleküler mekanizmayı incelemek için model organizma olarak *C. elegans*'ı kullandık. PHA ve PHB silyalarını fenotip ve uzunluk açısından incelemek için çok sayıda tekli, ikili ve üçlü mutantlar oluşturduk. Bir Joubert sendromu proteini olan ARL13B'nin, PHA & PHB silya ve ASE & ASI silyalarında silya yönünün belirlenmesinde gerekli olduğunu bulduk.

Anahtar kelimeler: Silya, BBS, PHA/PHB silya, silya-silya

Acknowledgements

I would like to thank my advisers, Dr Sebiha Çevik Kaplan and Dr Oktay İsmail Kaplan, for their precious support and guidance during my M.Sc. adventure. They provide an enjoyable lab atmosphere even if we have bad times like health problems, epidemics, and earthquakes. Numerous cheerful moments like drinking coffee, chatting between the experiments in the lab and lab's yard, lab activities, and exploring new routes are unforgettable for me. I want to thank all Kaplan Lab members, including Ferhan Yenisert, Atiyye Zorluer and Hanife Kantarcı, for supporting my experiments.

I want to thank my dear friend Mehmet Emin Orhan for accepting my collaboration offer, which provides a valuable friendship. Thank you for always standing with me. All the memories we have collected are precious.

I thank my daddy Coşkun Turan, mommy Havva Turan, Hasan Ali Turan and Fatmanur Turan for always believing in and supporting me.

TABLE OF CONTENTS

1. **INTRODUCTION 1**

1.1 CİLİA 1
1.2 CİLİA FORMATİON AND SUBCOMPARTMENTS 4
1.2.1 Basal Body (BB) 4
1.2.2 Transition Zone 4
1.2.3 Axoneme 5
1.2.4 Ciliary Membrane 5
1.3 INTRAFLAGELLAR TRANSPORT (IFT) 5
1.4 CİLİOPATHY 6

2. **MATERIALS AND METHODS 10**

2.1 MATERİALS 10
2.1.1 Strains 10
2.1.2 Primers and Plasmids 12
2.2 METHODS 13
2.2.1 Strains and Genetic Cross 13
2.2.2 Nematode Growth Medium (NGM) Preperation 15
2.2.3 Confocal Microscopy Imaging and Analysis Process 15
2.2.4 Dendrite Length Measurements 16
2.2.5 Stage Analysis 16
2.2.6 Plots and Statistical analysis 16

3. **RESULTS 18**

3.1 TWO DİSTİNCT CİLİA FROM TWO DİFFERENT SENSORY NEURONS JOİNTLY EXTEND 18
3.2 THE SMALL GTPASE ARL-13 İS ESSENTİAL FOR THE JOİNT CİLİA EXTENSİON OF PHA AND PHB 22
3.3 PARALLEL CILIA ELONGATION OF ASE AND ASI CILIA ELONGATION IS CONTROLLED BY THE SMALL GTPASES ARL-13 25
3.4 CİLİA LENGTH AND CİLİA DİRECTİON ARE İNDEPENDENT OF EACH OTHER 27
3.5 MİSDİRECTİON PHENOTYPE İNVESTİGATED İN *MKS-5 (TM3100); NPHP-4 (TM925)* AND *RPİ-1 (SYB722); NPHP-4 (TM925)* DOUBLE MUTANTS 29
3.6 MİSDİRECTİON OF *ARL-13(GK513); HDAC-6 (OK3203); NPHP-2(GK653)* TRİPLE MUTANT İS MORE FREQUENT THAN *ARL-13 (GK513)* SİNGLE MUTANT 31
3.7 THE BBSOME COMPONENT BBS-8 RESCUES THE CİLİA MİSDİRECTİON DEFECT OF ARL-13 33

4. **CONCLUSIONS AND FUTURE PROSPECTS 35**

4.1 CONCLUSIONS 35
4.2 SOCIETAL IMPACT AND CONTRIBUTION TO GLOBAL SUSTAINABILITY 37
4.3 FUTURE PROSPECTS 38

5. **BIBLIOGRAPHY** **39**
6. **APPENDIX** **45**
7. **CURRICULUM VITAE** **48**

LIST OF FIGURES

Figure 1.4. 1: Flagella-flagella interaction in the single-celled *Chlamydomonas*. 8

Figure 1.4. 2: The illustrations of a nematode *C. elagans* and cilia localizations. 9

Figure 2.2. 1: A genetic cross-process for generating one mutant with a fluorescent protein. 14

Figure 3.1. 1: Different cilia types show a similar communication pattern for the cilia elongation process. 20

Figure 3.1. 2: PHA and PHB cilia always come together from the early developmental stage. 21

Figure 3.2. 1: Joubert syndrome associated protein, ARL13B, is reguired for joint extension of PHA and PHB cilia. 24

Figure 3.3. 1: ARL13B is required protein for the parallel elongation of ASE and ASI cilia in amphid. 26

Figure 3.4. 1: The misdirection phenotype is not dependent on cilia length. 28

Figure 3.5. 1: The misdirection of PHA and PHB cilia is found in the *mks-5 (tm3100); nphp-4 (tm925)* and *rpi-1 (syb722); nphp-4 (tm925)* double mutants. 30

Figure 3.6. 1: *arl-13(gk513); hdac-6 (ok3203); nphp-2(gk653)* triple mutant has misdirection. 32

Figure 3.7. 1: BBS-8 partially rescues the misdirection phenotype of ARL-13. 34

LIST OF TABLES

Table 2.1.1. 1 Strain names and sources……. 10
Table 2.1.2. 1 Primer list..... 12

LIST OF ABBREVIATIONS

PCR	Polymerase Chain Reaction
NGM	Nematode Growth Medium
TEM	Transmission Electron Microscope
ssTEM	Serial Section Transmission Electron Microscope
JBTS	Joubert Syndrome
BB	Basal Body
TZ	Transition Zone

To my family…

Chapter 1

Introduction

The survivability of the organisms depends on understanding their environment, including the ability to smell potential food sources and avoid dangers. Due to the vast array of stimuli, organisms have had to create various sensory systems, including sensory neurons like cilia.

1.1 Cilia

Cilium, a singular form of cilia, is a hair-like appendage that extends from the cell surface and is a well-conserved organelle throughout evolution. The flagellum is an interchangeably useable term for cilia and shares a similar microtubule skeleton to cilia [1]. Cilia are found in almost every cell in the human body and are involved in embryo development [2], [3]. Additionally, cilia are responsible for the regulation and maintenance of the cells and are involved in different signaling pathways like the Hedgehog, Wnt, Hippo, and Notch [4]–[9].

Cilia are microtubule-based projections called axoneme surrounded by a ciliary membrane and are divided into two types: motile and non-motile (primary) cilia. The axoneme of motile cilia comprises nine doublets of microtubules forming a nine doublet microtubule ring around a central doublet (9+2), whereas primary cilia include nine doublets of microtubules without a central microtubule (9+0) [10]. Both types of cilia are preserved throughout evolution from single-celled organisms to human.

Motile cilia are mostly responsible for motility of cell and organism like sperm cell and single-cell green algae *Chlamydomonas reinhardtii,* respectively. Furthermore, left-right asymmetry in embryonic development, the movement of oocyte cells into fallopian tubes, and removing contaminations from the respiratory tract are all mediated by motile cilia [11]. In contradistinction to motile cilia, primary cilia are responsible for

sensing and signaling pathways. Primary cilia are responsible for mechanosensation, photosensation and chemosensation [12]–[14].

The morphological difference of cilia differs based on the function of the cell. For example, the olfactory cilia, referred to as tree-like cilia, locate in the respiratory system and provide the perception of odorants [15], [16]. Another one, kinocilium shows a staircase-like structure in ear cells and is found in both respiratory and auditory systems; however, it participates in the development of hair bundles [17]. The oviduct cilia seem like hair-like appendages in the mammalian reproduction system and are involved in the periodic transporting of eggs [18], [19]. Additionally, nodal cilia, photoreceptor connecting cilia, and kidney-collecting duct cilia have varied cilia structures that serve different duties based on human cell types [20].

The structure and subcompartments of primary cilia are evolutionarily conserved. The basal body (BB), axoneme, transition zone (TZ), and ciliary membrane are the main subcompartments involved in the primary cilia biogenesis (Figure 1. 1) [21]. The cilia term refers to the primary cilia throughout this thesis.

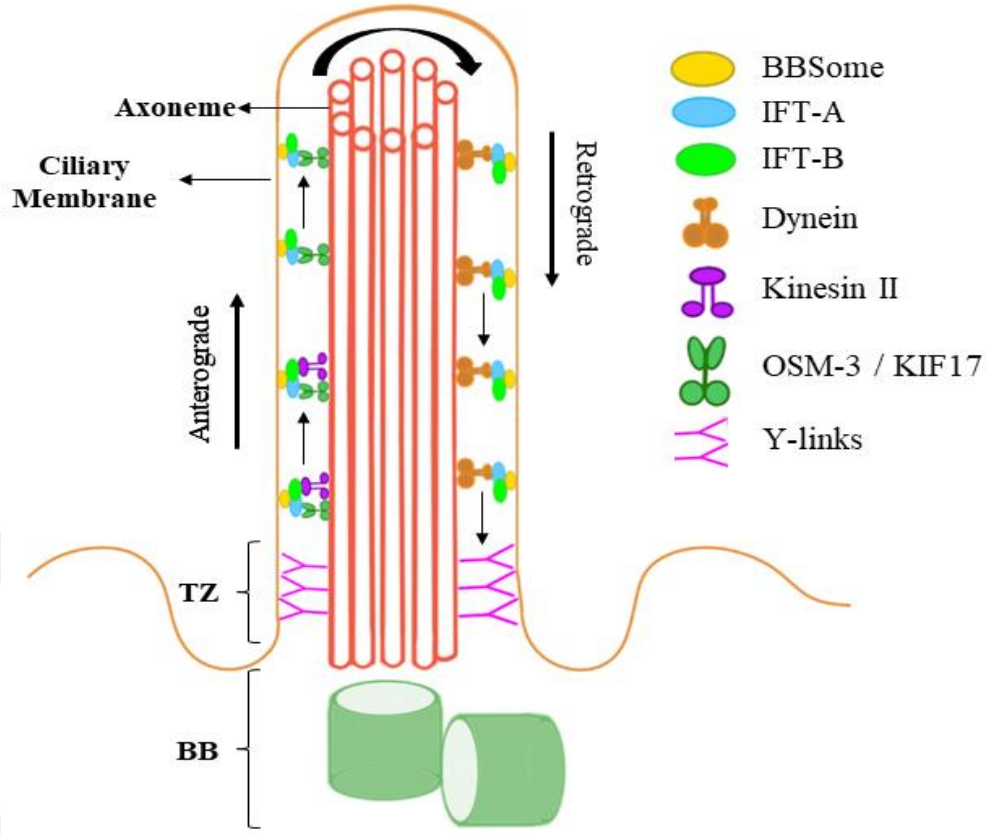

Figure 1. 1: The primary cilia structure and its components.

The primary cilium is composed of 9+0 axonemal structure which are encircled with ciliary membrane to constitute a cylindrical appendage. The intraflagellar transport (IFT) is ciliary molecule or signal delivery system throughout from the base of the cilia to ciliary tip, and vice versa. In the figure, the basal body and transition zone (with Y-shaped linkers) are marked using abbreviations BB and TZ, respectively. The Bardet-Biedl syndrome proteins, BBSome, and the IFT system subcomplexes, IFT-A and IFT-B, are also displayed. This figure is adapted from Turan M.G. and Orhan M.E. et al., 2022.

1.2 Cilia Formation and Subcompartments

1.2.1 Basal Body (BB)

The basal body is a modified centrosome which is located on the base of the cilia and constructs the primary cilia (Figure 1. 1). The initiation period of cilia construction is the G_0 (quiescence) or G_1 phases of the cell cycle [22]. The centrosome moving to the cell surface to differentiate into the basal body is the initial hallmark of ciliogenesis.

The centrosome consists of mother and daughter centrioles, and the mother and daughter centrioles are connected with fibers to form a centrosome. Two paired centrosomes are assembled in the S phase of the cell cycle and follow the G_2 phase for centriole elongation. Two paired centrioles are deconstructed at the end of G_2 or the beginning of M phases, and the oldest daughter centriole produces appendage proteins. After the M phase of the cycle, two paired centrioles are split, and the mother centriole moves along the membrane to construct the basal body and, eventually, the primary cilia. Mother centriole turns into the basal body; and the transition fibers and the subdistal appendages of the basal body get visible. The transition fibers provide a connection between the basal body and plasma membrane for initiating axonemal elongation. Then, the cilia formation process begins [23].

1.2.2 Transition Zone

The transition zone (TZ) is the intersection region between the end of the basal body and the axoneme base (Figure 1. 1). The nine-doublet structured TZ is linked to the ciliary membrane with Y-shaped linkers. It forms at the early stage of ciliogenesis and then guides to axoneme forming. TZ acts as a ciliary gate for selecting proteins (up to ~70 kDa) and allowing them to enter the cilia [24].

The ability of TZ to filter molecules can be originated from its two prominent subcomplexes, which are associated with the most known ciliopathies. Meckel Gruber syndrome (MKS) is one of them and consists of MKS1, MKS3 (TMEM67), MKS4 (CEP290), MKS8 (TCTN2), MKS9 (B9D1), MKS10 (B9D2), TMEM216, TCTN1, and TCTN3. The second complex is the nephronophthisis (NPHP) complex, including NPHP1, NPHP4, NPHP8, and NPHP2 proteins [25].

1.2.3 Axoneme

Axoneme is the microtubule-based cylindrical protrude extending from the base of the cilia (Figure 1. 1). Primary cilia comprise nine microtubule doublets, lacking a central microtubule (9+0). The nine doublets of microtubules in an axoneme are rooted from the triplet microtubule structure on the basal body/mother centriole. Each doublet covers two tubules, namely tubule A and tubule B. Tubule A and B differ in their protofilament composition, with tubule A comprising thirteen protofilaments and tubule B comprising ten protofilaments. Protofilaments are arranged tubulin dimers in a parallel direction to form cilia [26]. Protofilaments are called organized tubulin dimers in a parallel pattern to build axoneme [27].

1.2.4 Ciliary Membrane

The ciliary membrane is a specialized membrane that has undergone evolution and is used to encase axonemes. The ciliary membrane is derived from the plasma membrane with structural differences such as ion-binding capacity and distinctions in behavior under osmotic conditions [26]. Numerous signaling components are found within the ciliary membrane for regulating the transaction from the environment into the cilia and vice versa [28]. SMO, Patched1, and G-protein-coupled receptors (GPCRs) are important regulatory molecules that localize to the ciliary membrane [29].

1.3 Intraflagellar Transport (IFT)

The intraflagellar transport (IFT) system is a specialized particle and signal delivery system in the cilia. IFT mediates cellular signalling molecules and ciliary building blocks to construct a unique hair-like structure called cilia. In 1993, Kozminski KG. and colleagues discovered the IFT mechanism in unicelled *Chlamydomonas reinhardtii* by showing bidirectional movements of particles along the flagella using the differential contrast (DIC) microscopy [30]. IFT trains are responsible for transporting molecules from the base of the cilia to the tip of the cilia (anterograde) and vice versa (retrograde) for providing essential cilia formation processes and ciliary functions [31]. This anterograde and retrograde transport is named IFT. IFT molecules were biochemically isolated and characterized in 1998 in order to gain a better understanding

of the IFT system. Cole DG. and others identified kinesin-II motor protein and IFT-A and IFT-B complexes in flagella [32]. IFT-A and IFT-B complex proteins are determined with increasing technological advances in molecular biology.

IFT system consists of two multisubunit complexes for driving particle transportation: IFT-A and IFT-B. Anterograde transport is mediated by IFT-B complex powered with a kinesin-2 motor, while retrograde transport is moderated by IFT-A complex led with a dynein motor. IFT-A complex is composed of three core (IFT144, IFT140, and IFT122) and non-core (IFT139, IFT121, and IFT43) subunits. However, the IFT-B complex consists of 16 subunits by the association of six peripheral (IFT80, IFT38, IFT20, IFT54, IFT57, and IFT172) and ten core (IFT22, IFT25, IFT27, IFT46, IFT52, IFT56, IFT70, IFT74, IFT81, and IFT88) subunits [33]. In addition to IFT-A and IFT-B complexes, one octameric complex, the BBSome, is linked to IFT molecules. BBsome comprises eight subunits coded by most known BBS genes (BBS1, BBS2, BBS4, BBS5, BBS7, BBS8, BBS9, and BBS18) and provides a connection of IFT molecules to the ciliary membrane by linking IFT trains. BBSome controls the movement of particles out of the cilia [34]–[37] and is linked with the ciliary membrane [38].

1.4 Ciliopathy

Cilium, a singular term for cilia, is an evolutionarily conserved structure from unicellular organisms to humans by encountering various triggers and molecules. During their difficult evolutionary journey, the defects and dysfunctions of cilia or cilia-related compartments are connected to various human health problems called ciliopathy. Ciliopathy diseases are rare conditions originating from dysfunction and structural defect in cilia [39]. Fifty-five different ciliopathy is listed with variable clinical features in the literature [40]. Bardet–Biedl syndrome (BBS), Joubert syndrome (JBTS), nephronophthisis (NPHP), Meckel Gruber syndrome (MKS), polycystic kidney disease (PKD) are the most known ciliopathy diseases. Each ciliopathy has unique and common clinical features. For example, patients diagnosed with JBTS can present unique clinical features like bell-shaped chest, molar tooth sign, brainstem heterotopia and anteverted alae; however, polydactyly, anencephaly, ataxia, blindness, cleft lip and palate are common clinical features with other ciliopathies [40].

According to published articles in the literature, forty-four different genes are associated with JBTS, and most of the proteins (39 of 44) are localized in the ciliary subcompartments [40]. ARL13B (*arl-13* in *C. elegans*) is a well-known JBTS disease gene owing to its characteristic phenotype. ARL13B is one member of the ADP-ribosylation factor (Arf) protein family in mammals [41]. The Arf proteins are GTPases which are subgroups in the RAS protein family. These kinds of proteins are involved in various regulatory processes like the proliferation and differentiation of the cell. Managing cellular membranal flow is a crucial task the Arf protein family performs [42]. ARL13B is a required protein for the cilia formation process and is localized in the ciliary membrane [41], [43]. The ciliary axoneme of mouse cells has an abnormal phenotype compared to the wild-type in the absence of ARL13B protein [44]. Similar to this, this axonemal abnormality is seen in the different cilium types of *C. elegans* in the *arl-13* single mutant. PHA/PHB, AWB, and ASE cilia show abnormal axonemal elongation, called misdirection, without ARL13B protein in the worm [43].

Microorganisms consisting of cilia are excellent for modelling and understanding ciliopathy diseases in the laboratory. Cilia and cilia biogenesis can efficiently study in paramecium [45], *Chlamydomonas reinhardtii* [46] and *Tetrahymena thermophila* [47] as unicellular organisms or *Danio rerio* [48] and *Caenorhabditis elegans* [39] as multicellular model organisms. Cilia can be originated from different cell types and elongate together, or the same cell type can give a way to elongate multiple cilia. A single-celled green algae *Chlamydomonas* has two flagella which come from different basal bodies of a cell. Rosenbaum, JL et al. showed that both flagella are somehow interconnected to form the same flagella length. When one of the flagella is amputated, the intact flagellum shrinks to an equal length (Figure 1.4. 1) [49], [50].The two flagella depend on each other for determining their lengths, but it is hard to say how two flagella communicate with each other. Even though some specific interactions are defined in the literature, there is no clear explanation for flagella-flagella interactions.

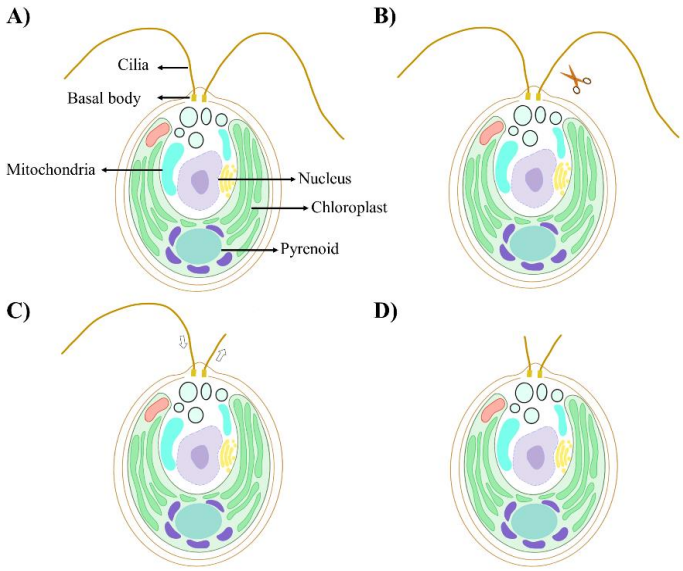

Figure 1.4. 1: Flagella-flagella interaction in the single-celled *Chlamydomonas*.

Representative drawing figures visualize the flagella-flagella interaction *Chlamydomonas* from A to D. A) *Chlamydomonas* contains two flagella that emerge from distinct basal bodies and extend outside the cell. B) When one flagellum is shortened, (C) the intact flagellum shrinks—the amputated flagellum stretches to come up the same length as the intact flagellum. D) In the end, both flagella come to the same length.

The interaction between cilia-cilia or flagella-flagella has not been thoroughly studied in the literature. The nematode worm *C. elegans* is a great fit organism to study cilia-cilia interaction because it contains several types of cilia in the head (amphid) and tail (phasmid) part of the worm (Figure 1.4. 2 A). The worm has 60 sensory neurons out of 302 neurons in hermaphrodites [51]. Eight different cilia are located in the amphid of the worm by elongating parallelly [52]. Specifically, this cilia bundle is called a ciliary channel which consists of ASE, ADF, ASG, ASH, ASI, ASJ, ASK, and ADL cilia [52]. In 2014, Doroquez, DB et al. used serial section transmission electron microscopy (ssTEM) to visualize distinct cilium types in *C. elegans* [52]. The different cilia types elongate in a parallel direction in the ciliary channel. For example, whereas ASE and ASI cilia initiate from different cell types, they simultaneously extend within the ciliary channel (Figure 1.4. 2 B) [52], [53]. In addition to the ciliary channel in the amphid, PHA and PHB cilia are located in the phasmid region of the worm (Figure 1.4. 2 C). PHA and PHB cilia originate from various cell types and join at the middle segment before simultaneously elongating into the ciliary tip. The transmission electron microscope (TEM) images of the phasmid region of the worm demonstrated that PHA and PHB cilia

are joined in the middle segment of them, and they are flush with each other to elongate into the end of the cilia [54].

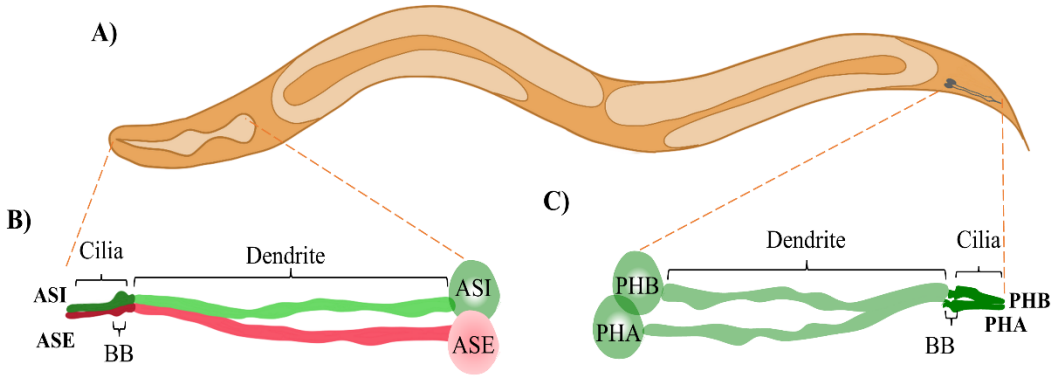

Figure 1.4. 2: The illustrations of a nematode *C. elagans* and cilia localizations.

A) A representative figure of *C. elegans* is given. B) ASE and ASI cilia originate from distinct cell types, are located in the ciliary channel in amphid and elongate parallelly. C) PHA and PHB cilia are located in the phasmid of the worm and elongate simultaneously by joining in the middle segment. (BB: Basal Body)

This thesis focused on investigating cilia-cilia interactions using *C. elegans* as a model organism. For this purpose, we analysed different cilia types, namely ASE/ASI and PHA/PHB, by measuring cilia length and classifying phenotypes as normal or misdirected (like *arl-13* single mutant) cilia, respectively.

Chapter 2

Materials and Methods

2.1 Materials

2.1.1 Strains

This thesis uses the following strains and mutants to generate single, double, and triple mutants (Table 2.1.1. 1).

Table 2.1.1. 1 Strain names and sources

STRAIN NAME	GENOTYPE	SOURCE
SP2101	osm-6(p811); mnIs17[osm-6::gfp; unc-36(+)	Blacque Lab
OIK27	*mks-2(nx111);* SP2101, osm-6(p811); mnIs17[osm-6::gfp; unc-36(+)	This work
OIK340	*mks-6(gk674);* SP2101, osm-6(p811); mnIs17[osm-6::gfp; unc-36(+)	This work
OIK154	*elmd-1(syb630);* SP2101, osm-6(p811); mnIs17[osm-6::gfp; unc-36(+)	This work
OH9671	otIs220 [gcy-5::mCherry] IV, otIs114 [lim-6p::GFP + rol-6(su1006)] I	CGC
CX3596	kyIs128 [str-3::GFP + lin-15(+)].	CGC
OIK1278	[OH9671, otIs220 [gcy-5::mCherry] IV, otIs114 [lim-6p::GFP + rol-6(su1006)] I + CX3596, kyIs128 [str-3::GFP + lin-15(+)]]	This work
OIK1279	*arl-13(gk513);* OIK1278, [OH9671, otIs220 [gcy-5::mCherry] IV, otIs114 [lim-6p::GFP + rol-6(su1006)] I + CX3596, kyIs128 [str-3::GFP + lin-15(+)]]	This work
EJP81	*vuaSi24 [pBP43; Pche-11::che-11::mCherry; cb-unc-119(+)]II; unc-119(ed3) III; che-11(tm3433) V*	Erwin J.G. PetermanLab
EJP501	vusSi001 ocr-2:eGFP IV.	Erwin J.G. PetermanLab
OIK1216	[EJP81, vuaSi24 [pBP43; Pche-11::che-11::mCherry; cb-unc-119(+)]II; unc-119(ed3) III; che-11(tm3433) V+EJP501, vusSi001 ocr-2:eGFP IV.]	This work
OIK1217	*arl-13(gk513);* OIK1216, [EJP,81, vuaSi24 [pBP43; Pche-11::che-11::mCherry; cb-unc-119(+)]II; unc-119(ed3) III; che-11(tm3433) V+EJP501, vusSi001 ocr-2:eGFP IV.]	This work
MX2418	*N2;nxEx1259[pbbs-8::PLC-delta PH::GFP;MKSR-2::tdTomato; coel::GFP]*	Leroux Lab
OIK1210	*arl-13(gk513);* MX2418, N2;nxEx1259[pbbs-8::PLC-delta PH::GFP;MKSR-2::tdTomato; coel::GFP]	This work
GOU2362	ift-74(cas499[ift-74::gfp]) II.	CGC
OIK997	*bbs-5(gk537) III.*; GOU2362, ift-74(cas499[ift-74::gfp]) II.	This work

OIK1151	*osm-12(bbs-7)*(ok1351) III.; GOU2362, ift-74(cas499[ift-74::gfp]) II.	This work
OIK1325	*hdac-6(ok3203);him-5(e1490);* GOU2362, ift-74(cas499[ift-74::gfp]) II.	This work
OIK1147	*mksr-1(tm3083)*; GOU2362, ift-74(cas499[ift-74::gfp]) II.	This work
OIK1220	*mks-5(tm3100)*; GOU2362, ift-74(cas499[ift-74::gfp])	This work
OIK1205	*dyf-5(ok1177) I.;* GOU2362, ift-74(cas499[ift-74::gfp])	This work
OIK1221	*nphp-2(gk653);* GOU2362, ift-74(cas499[ift-74::gfp])	This work
OIK1150	*nphp-4(tm925);* GOU2362, ift-74(cas499[ift-74::gfp]) II.	This work
OIK982	*kap-1(ok676)*; GOU2362, ift-74(cas499[ift-74::gfp])	This work
OIK983	*klp-13(tm3737)*; GOU2362, ift-74(cas499[ift-74::gfp])	This work
OIK1101	*W07G1.5(syb722)*(4X); GOU2362, ift-74(cas499[ift-74::gfp]) II.	This work
OIK1215	FX04910, *nekl-4(tm4910)*; GOU2362, ift-74(cas499[ift-74::gfp])	This work
OIK1232	*cdkl-1(ok2694);* GOU2362, ift-74(cas499[ift-74::gfp])	This work
OIK1263	*cep-104(C40H1.3(tur012)(*3X); GOU2362, ift-74(cas499[ift-74::gfp])	This work
OIK1334	DAM297, *ccep-290(tm4927) I*; GOU2362, ift-74(cas499[ift-74::gfp]) II.	This work
OIK1329	*ttll-4(tm3310);* GOU2362, ift-74(cas499[ift-74::gfp]) II.	This work
OIK1331	*ttll-11(gk482);* GOU2362, ift-74(cas499[ift-74::gfp]) II.	This work
OIK1372	*wdr-31(tm10423)*(4X); GOU2362, ift-74(cas499[ift-74::gfp]) II.	This work
OIK1333	F39H12.2(*wdr-54)(syb1005)*; GOU2362, ift-74(cas499[ift-74::gfp]) II.	This work
OIK1012	*arl-13(gk513);* GOU2362, ift-74(cas499[ift-74::gfp]) II.	This work
OIK964	*osm-3(p802);* GOU2362, ift-74(cas499[ift-74::gfp]) II.	This work
OIK1116	*W07G1.5(rpi-1)*(4X)*(syb722); nphp-4(tm925);* GOU2362, ift-74(cas499[ift-74::gfp])	This work
OIK1224	*nphp-4(tm925); mks-5(tm3100);* GOU2362, ift-74(cas499[ift-74::gfp])	This work
OIK1211	*arl-13 (gk513);* FX04910, *nekl-4(tm4910);* GOU2362, ift-74(cas499[ift-74::gfp])	This work
OIK1326	*hdac-6 (ok3203); nphp-2(gk653);* GOU2362, ift-74(cas499[ift-74::gfp]) II.	This work
OIK1324	*hdac-6 (ok3203); arl-13 (gk513);* ift-74(cas499[ift-74::gfp]) II.	This work
OIK1335	*osm-3(p802); arl-13 (gk513)*; GOU2362, ift-74(cas499[ift-74::gfp]) II.	This work
OIK1327	*arl-13(gk513); hdac-6 (ok3203); nphp-2(gk653);* GOU2362, ift-74(cas499[ift-74::gfp]) II.	This work
	N2; gmls13(srb-6p::GFP+pRF4)	Blacque Lab
OIK1226	*arl-13(gk513);* N2; gmls13(srb-6p::GFP+pRF4)	This work
OIK1338	*cdkl-1(ok2694);* N2; gmls13(srb-6p::GFP+pRF4)	This work
OIK1296	VC1130, ZK328.7(*ift-139)(gk508) III.*; N2; gmls13(srb-6p::GFP+pRF4)	This work
OIK1339	*cdkl-1(ok2694);arl-13(gk513);* N2; gmls13(srb-6p::GFP+pRF4)	This work
OIK1343	*arl-13(gk513);* VC1130, ZK328.7(*ift-139*)(*gk508*) III.; N2; gmls13(srb-6p::GFP+pRF4)	This work
OIK1337	*kap-1(ok676);* N2; gmls13(srb-6p::GFP+pRF4)	This work
OIK1298	*bbs-8(nx77);* N2; gmls13(srb-6p::GFP+pRF4)	This work
OIK1344	*ift-81(tm2355) X;* N2; gmls13(srb-6p::GFP+pRF4)	This work

OIK1336	*kap-1(ok676); arl-13(gk513*); N2; gmls13(srb-6p::GFP+pRF4)	This work
OIK1346	*bbs-8(nx77); arl-13(gk513);* N2; gmls13(srb-6p::GFP+pRF4)	This work
OIK1300	*ift-81(tm2355) X; arl-13(gk513);* N2; gmls13(srb-6p::GFP+pRF4)	This work

2.1.2 Primers and Plasmids

This thesis uses the following primers for Polymerase Chain Reaction (PCR) to generate double transgenics (Table 2.1.2. 1).

Table 2.1.2. 1 Primer list

	5' > 3' Sequence	
Genotype Name	**Forward**	**Reverse**
Primers		
arl-13(gk513)	gcatatggcgtcacaatgacc	cacaactccaacaaaaatgactcg
bbs-5(gk537)	ttgcatgaatgtaccacttgcgg	gaacctactcgcagggtgtc
bbs-8(nx77)	catgcaattgcctgaaacactg	gcaatgcttgtcggattcgac
ccep-290(tm4927)	ctgtacctggtctcgaaacgac	gcgtgctagaaattggtggtag
cdkl-1(ok2694)	gtgatcgaactgtacttcacg	ctgttccctcactgggtctc
cep-104(C40H1.3)(tur012)	TCTCCTTTCCATAGTAACAC	CAAGAAATGAACTGCCACAG
dyf-5(ok1177)	gagggaagactgagttgagtg	cgaaccttgtttgaactgccg
elmd-1(syb600)	CAACACACCCTCTCGCACAAC	GGAGCGCGATTGCATTGAAAC
F39H12.2(wdr-54)(syb1005)	ccagtaacgtactgctatac	CCTAGCGGGGCGAGTCC
hdac-6(ok3203)	AGTATGCCCAACACATCCG	AGTGAAGTCCGAGACGGAAA
ift-81(tm2355)	gctaaataacgagcgctatgc	aagaaaccctctgtcgtcattag
kap-1(ok676)	gctcgcttgagtgcttttgtatc	GTGGTACAAGACCTCCATTCACC
klp-13(tm3737)	gtcggagttgtactagtagaggac	gtcccgtcacgagtatcactc
mks-2(nx111)	aaaaaaccaacagaaccaggctgc	gtactatagcggtgcattccaac
mks-5(tm3100)	ttcctcttgcagcatagccaag	tccacagtaaccatcctttgttcc
mks-6(gk674)	GGGCGAAGAAAAATCCACATAATCC	TAACTTGTTGTGGCCATGCGC
mksr-1(tm3083)	gccggtaacattggatccac	ccgtccaatgtaggctatgc
nekl-4(tm4910)	cgatgcacaatgttttgggtgc	cgccatttccaacccaaaacc
nphp-2(gk653)	gacacgcaatcccattacac	gtaaactggagttataccag
nphp-4(tm925)	ccagcagcttgaaatagcag	gactgagaacattcgataccag
osm-12(bbs-7)(ok1351)	ctacagtacccccacagtgctc	cgttccacgtcaccagatacc
ttll-11(gk482)	TCAGAAGGCCCAAGTTTTTGGC	GCTGCAACGGTAAACTGAAC
ttll-4(tm3310)	AGCTCGTGGAACGGGAATTT	ccacaggggtggtaaacgat

W07G1.5(rpi-1)(syb722)	gaatgacgtggcttttcccaac	ggccatggcctagaaaccac
wdr-31(tm10423)	gtggtaccatagagctactg	CACCCCGAACTTGTGTCCATC
ZK328.7(ift-139)(gk508)	gttgaaccatggagccagagtg	TAGCATGCTTCTCCGTTGCTC

2.2 Methods

2.2.1 Strains and Genetic Cross

The Nematode Growth Medium (NGM) plates are used for maintaining strains at 20°C incubator, and strains are fed *Escherichia coli* OP50 bacteria by seeding on the plate surface [55].

The genetic cross is designed from Mendelian principles. Hermaphrodite and male *C. elegans* worms are used to tag with a fluorescent protein in one mutant background. To generate a single strain tagged with a fluorescent protein, wild-type males [38] are crossed with hermaphrodite worms with a marked fluorescent protein in drop agar plates. Hermaphrodites transfer agar NGM plates for the upcoming male offspring two days after fertilization (P_0 off), and male offspring are used for the new cross with a mutant in the next 2 or 3 days. These male worms have fluorescent protein. Then, male worms [38] and mutant hermaphrodite worms (5) cross in the drop plate. After two days, hermaphrodite worms transfer into new NGM agar plates for egg-laying and worm development. F1 generation is taken from one plate, which obtains high most male offspring. The target gene is heterozygote (+/-) for F1 generation worms; however, all worms do not have the fluorescent marker. For this reason, F1 clones take after the control of the marker using a microscope. F2 and further generations are followed by controlling both PCR and fluorescent markers (Figure 2.2. 1).

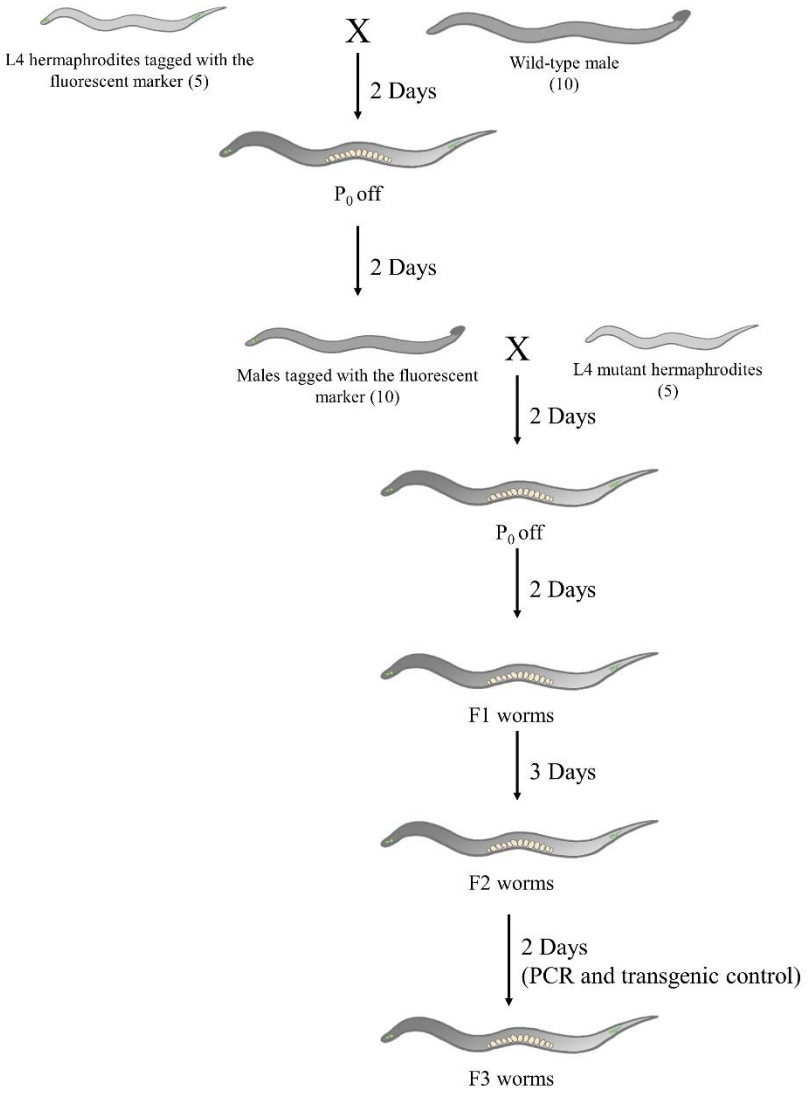

Figure 2.2. 1: A genetic cross-process based on Mendelian genetics principles.

The Mendelian cross principles are applied for generating single mutant with tagged fluorescent protein. Wild-type male (10) and larvae 4 (L4) stage hermaphrodite (5) worms are used for genetic cross and cross is followed by checking PCR and fluorescent protein. (P_0 refers to hermaphrodite parents of offspring; F1, F2, and F3 worms represent the following generations that come from P0.)

2.2.2 Nematode Growth Medium (NGM) Preperation

The nematode growth medium (NGM) agar plates use to cultivate *C. elegans* worms. NGM agar plates include 3 g NaCl, 2.5 g bacto peptone, and 17 g agar-agar in 1 L ddH_2O. Then, this mixture is sterilized using an autoclave up to 121°C. After sterilisation, the agar mixture is cooled to 50°C while being stirred with a magnetic stirrer. 1 mL nystatin (20 mg/mL), 1 mL cholesterol (5 mg/mL), 1 mL $MgSO_4$ (1 M), 1 mL $CaCl_2$ (1 M) and 25 mL KPO_4 (1 M) are added into an agar bottle in sterile conditions, and the mixture is stirred. Homogenized liquid agar is poured into petri dishes near a flame in the fume hood, and poured agar dishes stayed in the fume hood for 16 hours at room temperature. Following the day of agar pouring, 70 µl of *E. coli* OP50 bacteria grown in LB for 16 hours are spread on the plates and spread plates are left for 16 hours at room temperature for bacteria growth.

2.2.3 Confocal Microscopy Imaging and Analysis Process

In vivo imaging can be performed on worms that are healthy and well-fed. Before analysis day, plates are checked to ensure they contain adequate bacteria for worm feeding on NGM agar plates. Additionally, a few preparations are required to provide a proper analysis process at the beginning of confocal microscopy analysis. Before the start of an analysis, the room temperature stable is kept at 20°C, and 3% agarose in ddH_2O is prepared to mount worms for in vivo microscope analysis. An anaesthetizing reagent, 10 mM levamisole, is prepared from stock solution (500 mM) by diluting in M9 solution. After providing stable room temperatıre, a drop of 3% agarose is put to the slide and covered with another slide to form a straight surface. Then slides are gently seperated from each other without disintegrating agarose, and 2 µL of 10-20 mM levamisole is dropped into the agarose pad. Next, worms are transferred into levamisole using a platinum wire pick, and a cover slide is put over the worms under the stereomicroscope. The slide is placed into clips of the Zeiss LSM900 confocal microscope, and the ZEN 3 Blue edition software system is opened for taking Z-stack images using the Plan ApoChromat 63x/1.40 NA with 0.14 µm intervals. After collecting multiple Z-stack images, cilia lenght is measured using ZEN 3 Blue edition software. Cilia length is measured from the basal body to the end of the cilia for strains tagging with endogenous IFT-74::GFP transgenic. Alternatively, cilia length is measured from the periciliary

membrane compartment (PCMC) to the end of the cilia for strains tagging with SRB-6::GFP transgenic. In addition to cilia length analysis, cilia are grouped as normal or misdirected for determining the phenotypical difference between PHA and PHB cilia. During this analysis, the ZEN 3 Blue edition software is used for creating three-dimensional (3D) images from Z-Stack images.

2.2.4 Dendrite Length Measurements

Z-stack images are taken, which include cell body, dendrite, axon and cilia using wild-type, single and double mutant worms tagged with endogenous IFT-74::GFP transgenics under 40X magnification of LEICA compound microscope (LEICA DM6 B). The length of dendrite is measured from the middle of cell body to the distal end of the dendrite, not include transition zone and cilia. Andor software (Andor iQ 3.6.2) is used for measuring dendride lenght. A minimum of 15 dendrites are analyzed for each strain.

2.2.5 Stage Analysis

Stage analyses are made using healthy worms. The starvation of worms and contamination on the NGM agar plates or bacteria affect the health conditions of worms. Different stage worms, such as larva 1 (L1), larvae 4 (L4), 1-day, 5-day, and 8-day worms, are used to perform stage analyses. The L1 stage is the first developmental stage following egg-laying (9 hours), and L4 worms are developed at the 28th hour following hatching in 22°C [54]. L1 stage worms are analyzed in 9 hours after egg-laying. After then, L4-stage worms worms are analyzed. The analysis is continued with 1-day, 5-day, and 8-day worms. Worms are grown at 20°C, and the stages are analyzed under ZEISS LSM 900 confocal microscope.

2.2.6 Plots and Statistical analysis

The difference in the cilia structure was shown using bar plots. The ggplot2 [56] package was used to create bar plots, and the rstatix package (version 0.7.0) [57] was used to perform the Fisher's exact tests on the data to compare the two data sets. The cilia length, dendrite length and other length measurements were displayed with box plots. The ggplot2 library was used to construct box plots, while the rstatix library was utilized for performing statistical comparisons between each comparison. Specifically, T-test or

Wilcoxon paired test was used for comparison in the analysis. All analyses were performed in RStudio using R programming language (R version 4.1.2) [58].

Chapter 3

Results

3.1 Two distinct cilia from two different sensory neurons jointly extend

The 60 sensory neurons of 302 neurons in *C. elegans* are involved in sensing the environment and responding against the triggers, and these sensory neurons have disseminated both head (amphid) and tail (phasmid) parts of the worm. Most sensory cilia are located in the amphid of the worm by forming the ciliary bundle, called ciliary channel. They take signals and give cellular responses against foods, environmental stimulus, and chemicals.

ASE and ASI cilia are involved in a ciliary channel with six other cilia: ADF, ASG, ASH, ASJ, ASK, and ADL cilia. Specifically, ASE and ASI cilia are originated from distinct cell types and elongate in parallel directions to reach the mouth of the worm. Exhaustive images taken from TEM and ssTEM show their parallel elongation from basal bodies to tips [52], [54]. We generated a unique fluorescent marker for the vizualization of ASE and ASI cilia's structure in our laboratory. This marker is labelled ASE cilium with an str-3::GFP and ASI cilium with a gcy-5::mCherry fluorescent marker. The parallel elongation of ASE and ASI cilia is achieved using this double transgenic, as shown in Figure 3.1. 1 A.

After obtaining confocal images of ASE and ASI cilia in our lab, we investigated whether or not other cilia types follow similar cilia structure end of the elongation. Firstly, we decided to investigate PHA and PHB cilia, which are found in the phasmid of the worm (Figure 3.1. 1 B). PHA and PHB cilia extend their cilia separately from their dendritic ends. These cilia converge in the middle of the cilia and stretch together to the

tip of the cilia, giving the appearance of a single cilium. However, according to TEM pictures, the PHA and PHB cilia overlap after coming together, not joining [54].

We generated a special double transgenics by labelling IFT-A with CHE-11::mCherry [59] and the transmembrane calcium ion channel with OCR-2:eGFP [60]. Furthermore, PHA and PHB cilia are seen using endogenous single-copy IFT-74::GFP, an IFT-B member [61] (Figure 3.1. 1 C). Similar to the tendency of ASE and ASI cilia during elongation, PHA and PHB cilia elongate in the same direction even if they have different cilia lengths (Figure 3.1. 1 C). Remarkably, there was no statistically significant difference between PHA and PHB cilia when we measured the lengths of the PHA and PHB cilia separately (Figure 3.1. 1 D). Afterwards, we questioned the distance between the basal bodies of PHA and PHB cilia. We measured their positions and got a 0.48 μm distance for 32 cilia (Figure 3.1. 1 E). Briefly, the various cilia types in *C. elegans* exhibit similar phenotypic patterns at the end of the cilia elongation process, even if they come from different cell types.

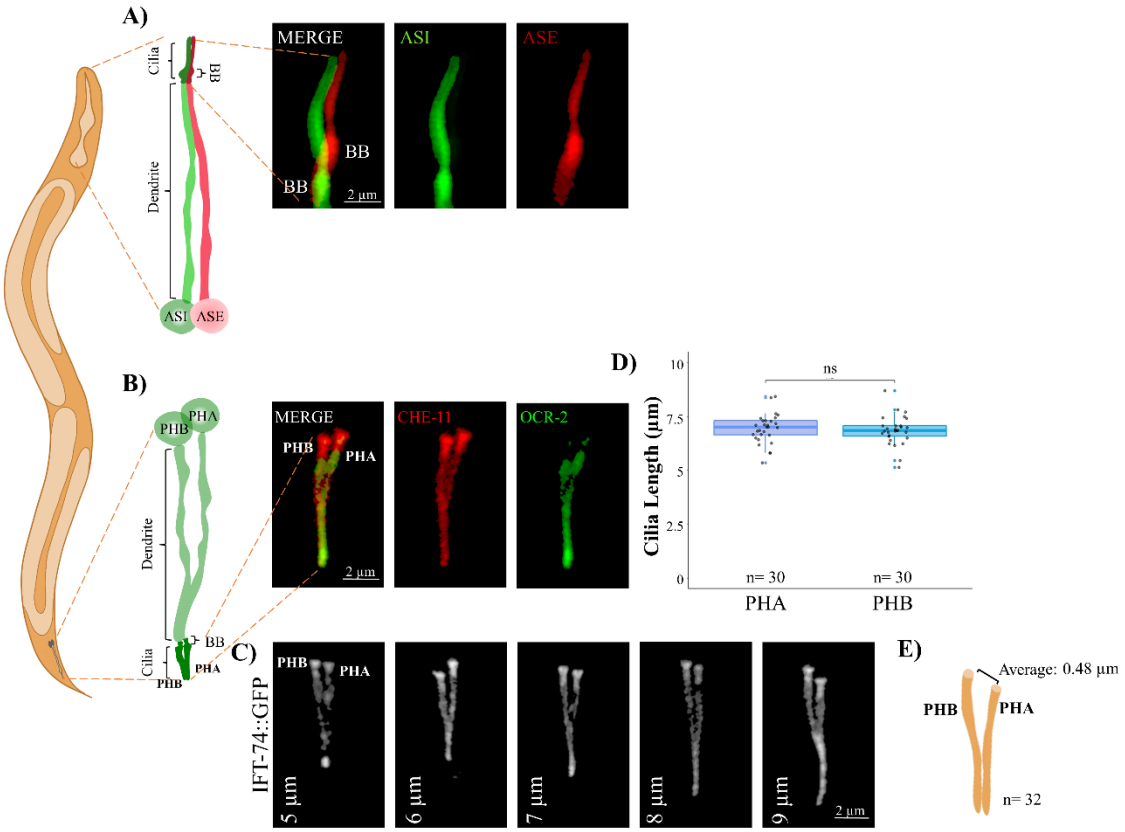

Figure 3.1. 1: Different cilia types show a similar communication pattern for the cilia elongation process.

A) The cilia structure for ASE and ASI is given horizontally in the representative and fluorescently marked images. ASE and ASI cilia originated from different cell bodies (given as green and red cycles) and followed their dendrites to elongate in a parallel direction from their basal bodies to ciliary tips. Dashed lines zoom to ASE and ASI cilia, tagged with str-3::GFP and gcy-5::mCherry fluorescent markers, respectively. B) The representative and fluorescently labelled photos horizontally display the cilia structure for PHA and PHB. They are located in the phasmid of the worm and come from different cell bodies (displayed with green cycles). CHE-11::mCherry and OCR-2:eGFP fluorescent markers are used to visualize PHA and PHB cilia in wild-type worms. C) The various ciliary lengths of wild-type worms are displayed using endogenous single-copy IFT-74::GFP fluorescent transgenics. D) PHA and PHB cilia lengths are not different from each other. The Wilcoxon two-paired statistical test is used to compare the individual lengths of the PHA and PHB cilia measured from the basal body to the cilium. E) The basal body position for each PHA and PHB cilia can be differ from each other even if they elongate simultaneously. BB indicates the basal body for each figure, and the scale bar is demonstrated with 2 µm for each fluorescent image.

The investigation of the cilia phenotype of PHA and PHB at diverse developmental stages revealed that they consistently intersected from the larvae 4 (L4) stage to the 8-day adult worm stage (Figure 3.1.2). This indicates that the regulation of cilia direction began prior to the L4 stage of worm development.

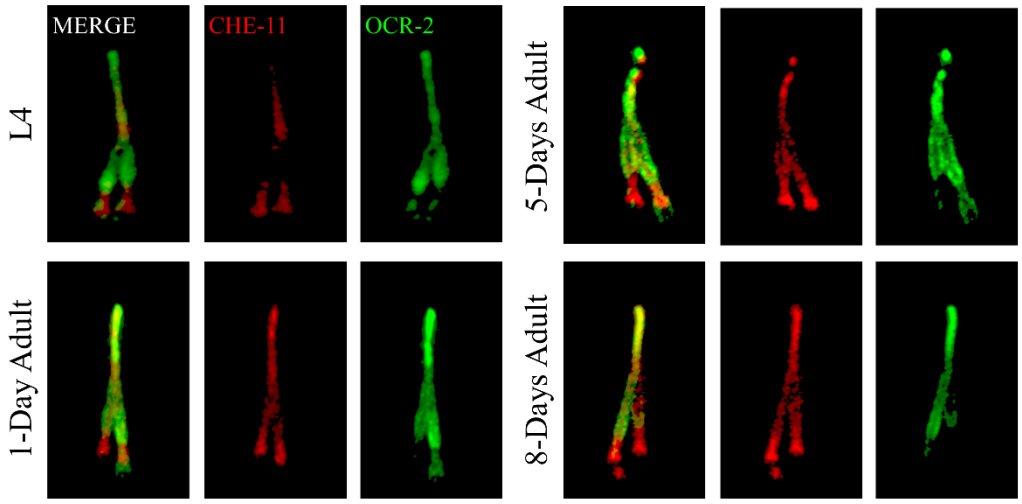

Figure 3.1. 2: PHA and PHB cilia always come together from the early developmental stage.

Wild-type worms tagged with CHE-11::mCherry; OCR-2:eGFP double transgenic are used for stage analysis (Larvae 4 (L4), 1-day, 5-days, and 8-days). A-D confocal images display PHA and PHB cilia structure from the L4 stage to 8-days adult worms. (Scale bar: 2 µm)

3.2 The small GTPase ARL-13 is essential for the joint cilia extension of PHA and PHB

PHA and PHB cilia come from different cell types and then elongate in parallel directions until the ciliary tip. The general cilia structure of PHA and PHB is usually similar in wild-type. We called this structure a Y-like structure or normal cilia throughout this thesis.

To investigate the cilia structure of PHA and PHB, we generated various single mutants, including *bbs-5 (gk537), bbs-7 (ok1351), hdac-6 (ok3203); him-5 (e1490), mksr-1 (tm3083), mks-2 (nx111), mks-5 (tm3100), mks-6 (gk674), dyf-5 (ok1177), nphp-2 (gk653), nphp-4 (tm925), kap-1 (ok676), klp-13 (tm3737), rpi-1 (syb722), nekl-4 (tm4910), elmd-1 (syb630), cdkl-1 (ok2694), cep-104 (tur012), ccep-290 (tm4927), ttll-4 (tm3310), ttll-11 (gk482), wdr-31 (tm10423), wdr-54 (syb1005), and arl-13 (gk513)* single mutants, labelling with endogenous IFT-74::GFP fluorescent protein and analyzed their structures under the confocal microscope. We selected those genes based on their cilia localization and ciliopathy associations. We selected several proteins for phenotype screening, including basal body proteins (BBS-5, BBS-7, and MKS-2), transition zone proteins (NPHP-4, MKSR-1, MKS-5, MKS-6 and CDKL-1), ciliary proteins (CEP-104, WDR-31, NPHP-2, DYF-5, TTLL-4, NEKL-4, and RPI-1), and ciliary membrane protein (ARL-13) [40], [62]–[64]. Additionally, KAP-1 and KLP-13 were chosen due to their kinesin roles [65], and TTLL-11 was preferred for the glutamylation activity in the microtubule [66]. CCEP-290 is a centred protein at the microtubule cylinder of the transition zone [67]. HDAC-6 is a deacetylase that mediates the differentiation of glioma cells using cilia [68]. Lastly, WDR-31 and ELMD-1 were selected for being new cilia-associated genes [64].

Figure 3.2.1 A shows that twenty-two single mutants exhibit normal cilia phenotypes similar to wild-type, even with different cilia lengths. The *arl-13* single mutant is an exception since it has a unique structure. As seen in the panel, PHA and PHB cilia come together in the middle, then elongate until the tip of cilia them (displayed with * in the panel). However, the PHA and PHB cilia do not come together to elongate concurrently in the absence of ARL-13 protein and instead pursue distinct paths (called misdirected cilia, ** displays the tips of PHA and PHB cilia). Then, we deciaded to visualize PHA and PHB cilia using different fluorescent markes which are CHE-

11::mCherry; OCR-2:eGFP and PLC::GFP; MKSR-2::tdTomato (Figure 3.2. 1 B). The *arl-13* single mutant displays a misdirection phenotype when labelled using different ciliary and cellular fluorescent proteins.

To ensure the distribution of normal and misdirection phenotypes in the single mutants, we analyzed their cilia structure by counting at least 10-15 worms (Figure 3.2. 1 C) In the absence of ARL-13 and MKS-5 proteins, the misdirection phenotype is statistically meaningful compared to the wild-type (We focued *arl-13* gene in the rest of analyzes.). Additionally, we individually measured PHA and PHB cilia length for each strain (Figure 3.2. 1 D). Even if single mutants have shorter or longer cilia than wild-type, their cilia structure is normal (except for *arl-13*).

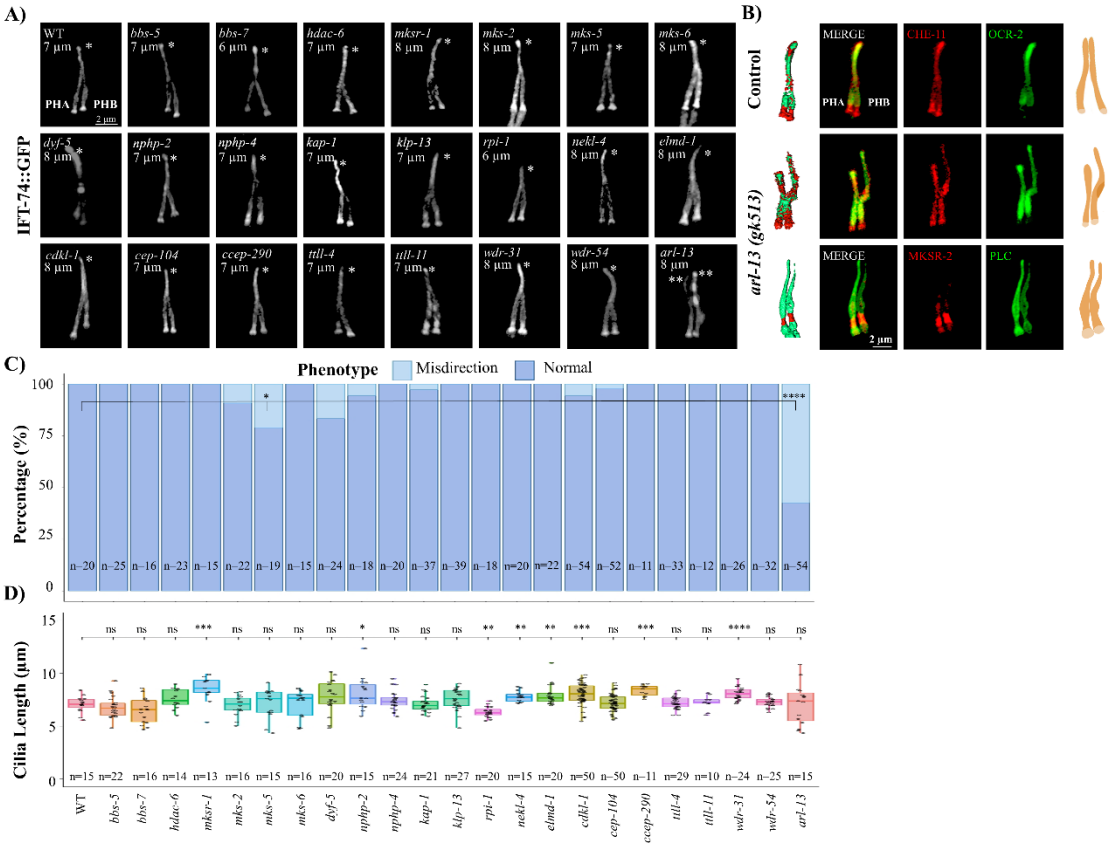

Figure 3.2. 1: Joubert syndrome associated protein, ARL13B, is reguired for joint extension of PHA and PHB cilia.

A) *arl-13 (gk513)* single mutant has unique pheotype than other mutants.The panel indicates the PHA and PHB cilia lengths and structures in wild-type and other single-mutant worms tagged with single-copy OSM-6::GFP and endogenous single-copy IFT-74::GFP fluorescent transgenics. Panel consists of *bbs-5 (gk537), bbs-7 (ok1351), hdac-6 (ok3203); him-5 (e1490), mksr-1 (tm3083), mks-2 (nx111), mks-5 (tm3100), mks-6 (gk674), dyf-5 (ok1177), nphp-2 (gk653), nphp-4 (tm925), kap-1 (ok676), klp-13 (tm3737), rpi-1 (syb722), nekl-4 (tm4910), elmd-1 (syb630), cdkl-1 (ok2694), cep-104 (tur012), ccep-290 (tm4927), ttll-4 (tm3310), ttll-11 (gk482), wdr-31 (tm10423), wdr-54 (syb1005),* and *arl-13 (gk513)* single mutants, respectively. * and ** indicate ciliary tip in the panel, and the scale bar is present 2 µm. B) In the absence of ARL-13 protein, PHA and PHB cilia are misdirected. PHA and PHB cilia are visualized using CHE-11::mCherry; OCR-2:eGFP and PLC::GFP; MKSR-2::tdTomato fluorescent markers in wild-type (top of the panel) and *arl-13 (gk513)* (middle and bottom of the panel) single mutants. 3D structures (left column in the panel), taken from confocal microscope, and representative images (right column in the panel) are given for wild-type and *arl-13 (gk513*) single mutant. C) The misdirection phenotype is statistically significant in *arl-13 (gk513)* and *mks-5 (tm3100*) single mutants. The phenotypic distribution of PHA and PHB cilia are classified as normal and misdirection, and the percentage for each mutant is given in the bar graph. The normal and misdirected phenotypes of single mutations and wild-type are compared using Fisher's exact test (*= 0.05, ****=0.0001). D) Cilia length is measured from the basal body to the tip of the cilia for wild-type and every single mutant (Given PHA cilia length). Cilia length for each mutant is statistically compared with wild-type, and results are given in the boxplot using * and ns. (Wilcoxon paired-two test, ****=1e-04, ***= 0.001, **=0.01, *=0.05, ns =not significant)

3.3 Parallel cilia elongation of ASE and ASI cilia elongation is controlled by the small GTPases ARL-13

ASE and ASI cilia are two types of cilium located in ciliary channels in the amphid region of *C. elegans*. They support chemosensation and thermosensation by being directly exposed to the environment [69].The focused ion beam scanning electron microscopy (FIB-SEM) and serial section transmission electron microscopy (ssTEM) microscope images indicate that these long slender ASE and ASI cilia originate from different origins and elongate to achieve the mouth of the worm [52], [53]. This elongation occurs in a parallel direction.

To visualize ASE and ASI cilia, we generated a []double transgenic marker by tagging ASE cilia with gcy-5::mCherry and ASI cilia with str-3::GFP (Figure 3.3. 1 A). Similar to the literature review about the linear elongation of ASE and ASI cilia, we obtained a similar result using double transgenic in the wild-type worms: ASE and ASI cilia are elongated in the same direction. Nevertheless, ASE and ASI cilia are misdirected without ARL-13 protein (Figure 3.3. 1 B). The misdirection phenotype of the *arl-13 (gk513)* single mutant is statistically different compared to the wild-type. In brief, ARL-13 is the required for regulating the direction of the ASE and ASI cilia during the elongation process **(**Figure 3.3. 1 C).

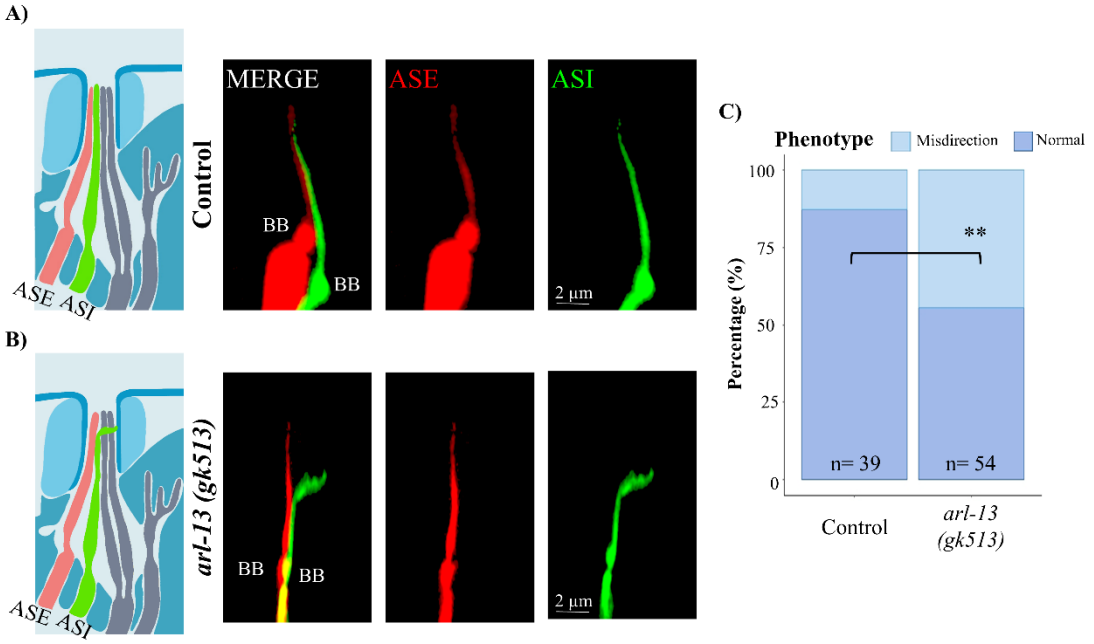

Figure 3.3. 1: ARL13B is required protein for the parallel elongation of ASE and ASI cilia in amphid.

ASE and ASI cilia elongate from different basal bodies in a parallel direction. A) ASE and ASI cilia elongation is shown in the representative figure and wild-type worm using gcy-5::mCherry for ASE and with str-3::GFP for ASI cilia. B) Misdirection is observed in *arl-13 (gk513)* single mutant tagging with gcy-5::mCherry and str-3::GFP double transgenics. C) Misdirection phenotype of *arl-13 (gk513)* single mutant is statistically significant than wild-type. Fisher's exact test is applied when comparing normal and misdirection phenotypes for wild-type and *arl-13 (gk513)* single mutant worms tagging with gcy-5::mCherry and str-3::GFP (**= 0.01). (Scale bar: 2 µm)

3.4 Cilia length and cilia direction are independent of each other

To better understand the relationship between the cilia length and cilia structure, various double mutants, namely *arl-13 (gk513); cdkl-1 (ok2694), arl-13 (gk513); ift-139 (gk508),* and *arl-13 (gk513); nekl-4 (tm4910),* are generated. Cilia structures were categorized as normal and misdirected (given in Figure 3.4. 1 C) for every single and double mutant. Subsequently, a comparison is made between the phenotypical differences exhibited by the wild-type vs the single/double mutant and the single vs double mutant for each double mutant (Figure 3.4. 1 A). Similar to previous results given in Figure 3.2.1 and Figure 3.3.1, *arl-13 (gk513)* single mutant has misdirection phenotype than others. Additionally, *arl-13 (gk513); cdkl-1 (ok2694)*, *arl-13 (gk513); ift-139 (gk508)*, and *arl-13 (gk513); nekl-4 (tm4910)* double mutants have statistically significant misdirection phenotype when comparing with wild-type and their single mutants *(cdkl-1 (ok2694), ift-139 (gk508),* and *nekl-4 (tm4910))* except *arl-13 (gk513)* single. However, there is no statistically noticeable phenotypic difference between *arl-13 (gk513)* single vs double mutants. This means the misdirection phenotype of double mutants stems from the absence of the ARL-13.

In addition to phenotype analysis, we measured the length of PHA cilium for each strain, and the analysis compared wild-type, single and double mutants (Figure 3.4. 1 B). The *arl-13 (gk513); ift-139 (gk508)* double mutant displayed a statistically significant reduction in cilia length compared to the wild-type. In contrast, the double mutants of *arl-13 (gk513); nekl-4 (tm4910)* exhibited a statistically significant increase in cilia length compared to the wild-type. However, *arl-13 (gk513); cdkl-1 (ok2694)* double mutants do not have any statistically meaningful difference from the wild-type. In short words, misdirection phenotype and cilia length is regulated independently.

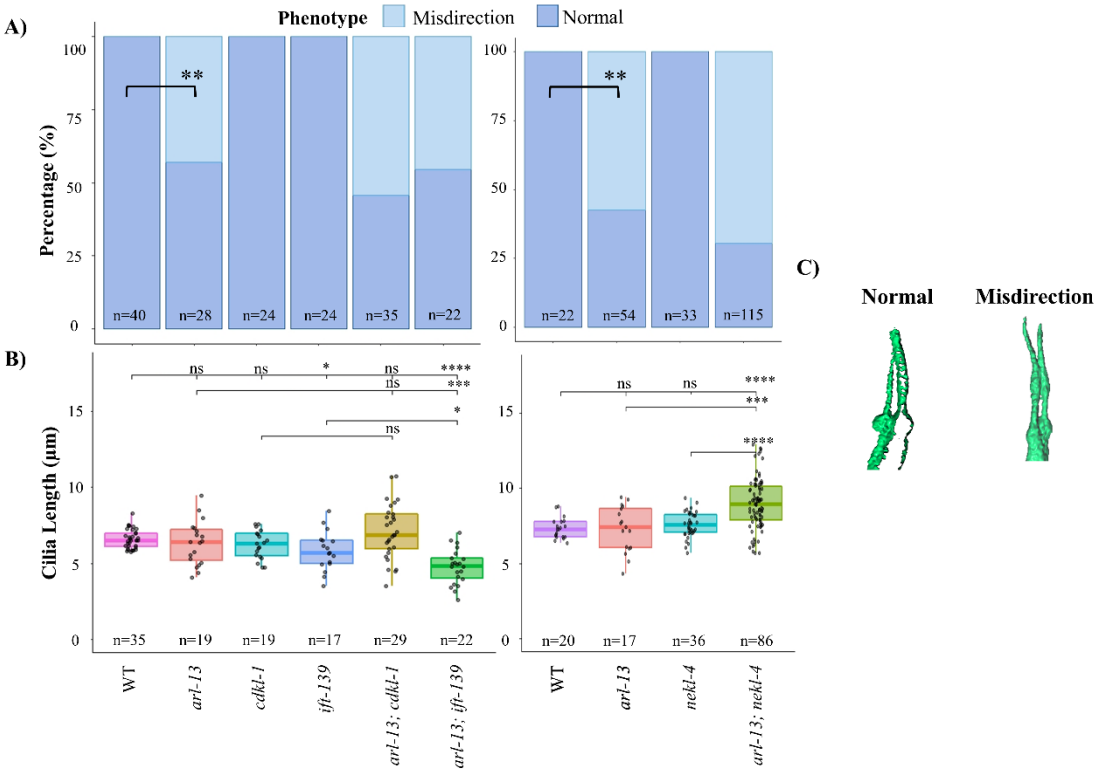

Figure 3.4. 1: The misdirection phenotype is not dependent on cilia length.

A) The misdirection phenotype seen in double mutants is due to the lack of the ARL-13 protein. *arl-13 (gk513); cdkl-1 (ok2694)* and *arl-13 (gk513); ift-139 (gk508)* double mutants and their single mutants (*arl-13 (gk513), cdkl-1 (ok2694),* and *ift-139 (gk508)*) have been labeled with SRB-6::GFP, while the double mutant of *arl-13 (gk513); nekl-4 (tm4910)* and its singles (*arl-13 (gk513), nekl-4 (tm4910)*) have been marked with a single-copy endogenous IFT-74::GFP fluorescent marker. The bar graphs with exact worm numbers (n) show the percentages of normal and misdirection cilia for each strain. Normal and misdirection phenotype is analyzed using Fisher's exact test (**= 0.01). B) Cilia length is independent of cilia phenotype in *arl-13 (gk513); cdkl-1 (ok2694)*, *arl-13 (gk513); ift-139 (gk508)* and *arl-13 (gk513); nekl-4 (tm4910)* double mutants, even if they have shorter or longer cilia than wild-type. The box plot includes the statistical outcomes of comparing the PHA cilia length between strains. (n stands for worm number.) (Wilcoxon paired-two test is applied, ****=1e-04, ***= 0.001, **=0.01, *=0.05, ns =not significant) C) Normal and misdirection cilia are given in 3D representative forms taken from the confocal microscope.

3.5 Misdirection phenotype investigated in *mks-5 (tm3100); nphp-4 (tm925)* and *rpi-1 (syb722); nphp-4 (tm925)* double mutants

A recently published paper from our laboratory shows that the basal body (BB) position of PHA and PHB cilia in the *rp-1 (syb722); nphp-4 (tm925)* double mutant can be positioned at different points [62]. Then we considered that the direction of PHA and PHB cilia can be outcome from the different positioned of their BB. To investigate this hypothesis, we analysed this double mutant as well as *mks-5 (tm3100); nphp-4 (tm925)* double mutant.

The initial analysis involves the determination of the phenotypic distinction between double mutants and wild-type (Figure 3.5. 1 A). *rp-1 (syb722), nphp-4 (tm925), mks-5 (tm3100), arl-13 (gk513)* single and *mks-5 (tm3100); nphp-4 (tm925), rp-1 (syb722); nphp-4 (tm925)* double mutants are categorised in normal, and misdirection groups and this groups are statistically compared for each mutant. Statistical analysis indicates that *mks-5 (tm3100); nphp-4 (tm925)* and *rp-1 (syb722); nphp-4 (tm925)* double mutants exhibit a misdirection phenotype in comparison to the wild-type worms and single mutants. Then, we measured PHA cilia lenghts for wild-type and each mutant (Figure 3.5. 1 B). The confocal images demonstrate that BBs of PHA and PHB are undoubtedly positioned differently in *mks-5 (tm3100); nphp-4 (tm925)* and *rp-1 (syb722); nphp-4 (tm925)* double mutants (Figure 3.5. 1 C, BB is marked with *).

To clarify the effect of BB positions on PHA and PHB cilia direction, we analyzed two main things: the BB distance between PHA and PHB cilia and their dendrite lengths **(**Figure 3.5. 1 D**)**. The BB distance is statistically wider in *mks-5 (tm3100); nphp-4 (tm925)* and *rp-1 (syb722); nphp-4 (tm925)* double mutants than in single mutants (Figure 3.5. 1 E). Additionally, dendrite lengths for each strain is measured from the cell body to the BB and anlaysed (Figure 3.5. 1 F). Briefly, these mutants have shorter dendride length than wild-type.

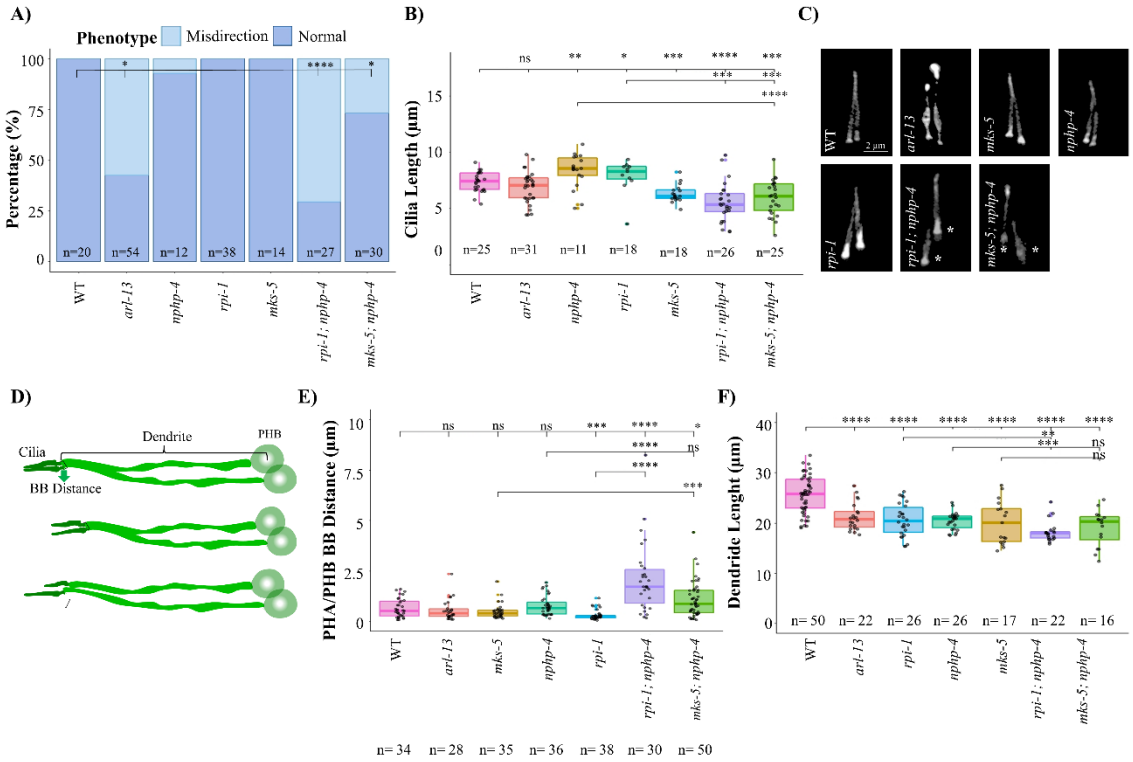

Figure 3.5. 1: The misdirection of PHA and PHB cilia is found in the *mks-5 (tm3100); nphp-4 (tm925)* and *rpi-1 (syb722); nphp-4 (tm925)* double mutants.

rpi-1 (syb722); nphp-4 (tm925), mks-5 (tm3100); nphp-4 (tm925) double and *arl-13 (gk513), nphp-4 (tm925), rpi-1 (syb722), mks-5 (tm3100)* single mutants are labelled with single-copy endogenous IFT-74::GFP fluorescent protein. A) The percentages pertaining to the PHA and PHB cilia structure for each mutant have been provided. Statistical analysis indicated that *rpi-1 (syb722); nphp-4 (tm925) and mks-5 (tm3100); nphp-4 (tm925)* double mutants and *arl-13 (gk513)* single mutant display misdirection phenotype than wild-type. (Fisher's exact statistical test, **= 0.01, ****=0.0001) B) The PHA cilia lengths of strains are measured from the basal body to the tip of the cilia and compared using the Wilcoxon paired statistical test between single and double mutants. C) Representative confocal images are given in the panel. (Scale bar: 2 µm, * shows the basal body positions for PHA and PHB.) D) The illustrations show PHA and PHB cilia extending from their cell bodies to their tips. Based on the basal body (BB) positions, cilia length can be changed. E) The BB positions between PHA and PHB cilia are measured for each strain and statistical analysis (Wilcoxon paired statistical test) is applied for comparision. F) The dendride length of each strain is measured from the center of cell body to the basal body, and then each double mutant is analysed with its single mutants appliying Wilcoxon paired statistical test. (****=1e-04, ***= 0.001, **=0.01, *=0.05, ns =not significant) (n represents the cilia number used for analysis.)

3.6 Misdirection of *arl-13 (gk513); hdac-6 (ok3203); nphp-2 (gk653)* triple mutant is more frequent than *arl-13 (gk513*) single mutant

We wondered how other double or triple mutants with *arl-13* can affect the PHA and PHB cilia direction. In pursuit of this objective, we thoroughly examined scholarly articles related to ARL13B/arl-13. Warburton-Pitt, Simon R F and colleagues presented the dye assay results of the *arl-13(gk513); hdac-6 (ok3203); nphp-2(gk653)* triple mutant [70]. We considered that the PHA and PHB cilia structure of this triple could be suitable for our research perspective and involved in the cilia phenotype and length analysis.

PHA and PHB cilia direction and length are detailed investigated for *arl-13(gk513), hdac-6 (ok3203), nphp-2(gk653)* single; *arl-13(gk513); hdac-6 (ok3203), arl-13(gk513); nphp-2(gk653), arl-13(gk513); nphp-2(gk653)* double and *arl-13(gk513); hdac-6 (ok3203); nphp-2(gk653)* triple mutants (Figure 3.6. 1). PHA and PHB cilia structure is classified into normal and misdirection groups, and *arl-13(gk513); hdac-6 (ok3203); nphp-2(gk653)* triple mutant is statistically compared with double mutants (Figure 3.6. 1 A). Suprisingly, the misdirection phenotype is more severe than *arl-13 (gk513)* single mutant. Additionally, we measured cilia length of PHA cilia in each mutant and compared them (Figure 3.6. 1 B). The PHA cilia length of this triple mutant is statistically shorter than the wild-type, single and double mutants. The panel in Figure 3.6. 1 C contains representative confocal images for each mutant. In addition to these analyses, we did not involve the *arl-13(gk513); nphp-2(gk653)* double mutant in phenotype and length analyses due to tiny PHA and PHB cilia.

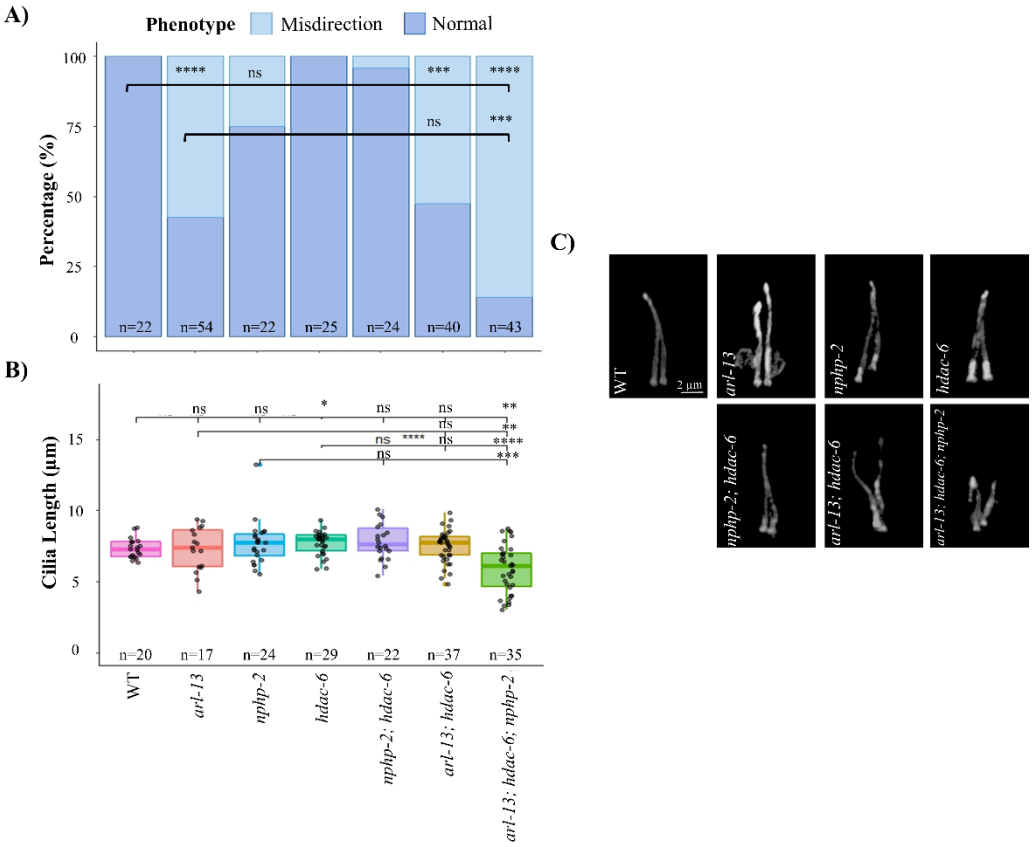

Figure 3.6. 1: *arl-13(gk513); hdac-6 (ok3203); nphp-2(gk653)* triple mutant has misdirection.

A) *arl-13(gk513); hdac-6 (ok3203); nphp-2(gk653)* triple mutant tagged with single-copy endogenous marker, IFT-74::GFP, has severe phenotype than *arl-13 (gk513)* single mutant. PHA and PHB cilia direction is classified into normal and misdirection groups for wild-type, *arl-13(gk513), hdac-6 (ok3203), nphp-2(gk653)* single*; arl-13(gk513); hdac-6 (ok3203), arl-13(gk513); nphp-2(gk653)* doubles *and arl-13(gk513); hdac-6 (ok3203); nphp-2(gk653)* triple mutants. Statistical analysis of each comparison group (wild-type vs singles/doubles/triple, doubles vs triple) shows that the misdirection phenotype of *arl-13(gk513); hdac-6 (ok3203); nphp-2(gk653)* triple mutant is more severe than *arl-13 (gk513)* single mutant. (Fisher's exact test, ****=0.0001) B) *arl-13(gk513); hdac-6 (ok3203); nphp-2(gk653)* triple mutant has shorter PHA cilia than *arl-13 (gk513)* single mutant. Each cilia length of PHA is measured and presented with statistical results in the box plot (Wilcoxon paired test is applied, ****=1e-04, ***= 0.001, **=0.01, *=0.05, ns =not significant). C) Representative cilia structures of mutants are given in the panel (Scale bar: 2 µm).

3.7 The BBSome component BBS-8 rescues the cilia misdirection defect of ARL-13

The role of essential ciliary genes such as kinesins, the IFT complex, and BBSome in controlling the PHA and PHB cilia's direction was the following question we considered. Therefore, we targeted essential genes related to a complex or subunit for comprehing the misdirection phenotype in double mutants with *arl-13 (gk513).* We selected *bbs-8 (nx77)* due to its belonging to the BBSome complex [71], *osm-3 (p802)* due to being an essential homodimeric motor protein [72], *kap-1 (ok676)* due to being a kinesin and a linker between the IFT motor and cargo [73], and *ift-81 (tm2355)* due to being a member of the IFT-B complex [33] in primary cilia. Subsequently, an analysis is conducted on the phenotypical differences and cilia length of the PHA and PHB cilia of *arl-13 (gk513); kap-1 (ok676), arl-13 (gk513); bbs-8 (nx77),* and *arl-13 (gk513); ift-81 (tm2355)* double mutants with their single mutants (Figure 3.7. 1).

The phenotypic analysis of double mutants with *arl-13 (gk513)* demonstrated no significant difference between single and double mutants except *arl-13 (gk513); bbs-8 (nx77)* double mutant. Interestingly, the *arl-13 (gk513); bbs-8 (nx77)* double mutant displayed a decrease in misdirection and an increase in normal phenotype compared to the *arl-13 (gk513)* single mutant, as confirmed by statistical analysis (Figure 3.7. 1A/B). This indicates that BBS-8 and ARL-13 are regulatory proteins that control cilia direction. Furthermore, *arl-13 (gk513); osm-3 (p802)* double mutant has shorter cilia which do not intersect in the middle of PHA and PHB cilia. For this reason, we did not evaluate this double in the phenotype and length analysis.

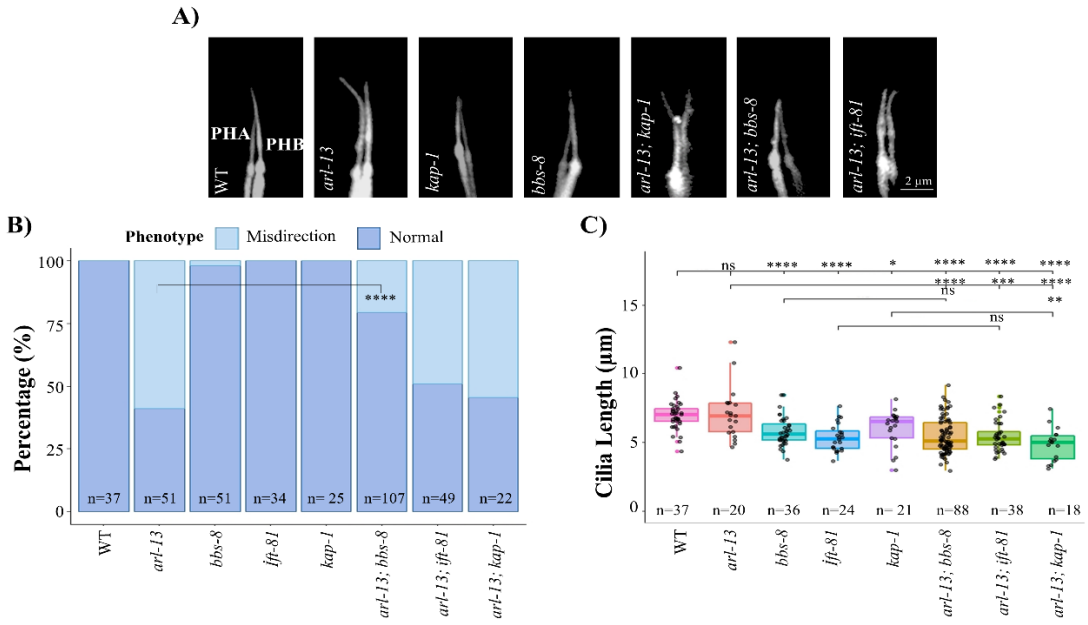

Figure 3.7. 1: BBS-8 partially rescues the misdirection phenotype of ARL-13.

A) The panel displays the cilia structures of PHA and PHB cilia of wild-type and mutants, which are *arl-13 (gk513), kap-1 (ok676), bbs-8 (nx77)* single, *arl-13 (gk513); kap-1 (ok676), arl-13 (gk513); bbs-8 (nx77),* and *arl-13 (gk513); ift-81 (tm2355)* double mutants. (Scale bar: 2 µm) B) The misdirection phenotype is more severe in *arl-13 (gk513)* single mutant than *arl-13 (gk513); bbs-8 (nx77)* double mutant. The cilia structure of PHA and PHB for each mutant is categorized into the normal and misdirected groups, as indicated in the bar plot. To compare phenotypical groups, Fisher's exact test is applied (****=0.0001). C) PHA cilia lengths of each mutant are measured from the basal body to the end of the cilia. The box plot is displayed cilia length and statistical results between mutants (Wilcoxon paired-two test is used for comparing groups, ****=1e-04, ***= 0.001, **=0.01, *=0.05, ns =not significant). (n used for noting the worm numbers used in this analysis.)

Chapter 4

Conclusions and Future Prospects

4.1 Conclusions

The primary cilia, the plural form of the cilium, are microtubuled sensory neurons which are protruded from the cell surface to the outside. Cilia arise from the cell body by following dendrites to achieve forming own structure. Various types of cilia can arise from different cell types, whereas some cilia share the same cell to occur. For example, the single-celled *Chlamydomonas* has two flagella which come from the same cell and are interconnected with each other [49], [50]. Additionally, the nematode *C. elegans* has various cilia, such as ASE, ASI, PHA, and PHB cilia originating from different cell types. TEM [53] and ssTEM [52] images revealed that ASE, ASI, PHA, and PHB cilia come from different cell types, and ASE & ASI and PHA & PHB cilia elongate in a parallel direction. However, there is a mystery in explaining the parallel cilia elongation.

In this thesis, we examined how cilia direction is determined. For this purpose, we used the nematode *C. elegans* as a model organism in our laboratory. Firstly, we target to analyze ASE and ASI cilia labelled with unique transgenics. ASE and ASI cilia showed parallel elongation in the amphid. However, the amphid of the worm is more mobile than the phasmid, and this mobility causes a complicated analysis process. Therefore, we decided to analyze PHA and PHB cilia located in the phasmid throughout the rest of the detailed analysis.

We generate twenty-three single mutant and analyzed their PHA and PHB cilia structure. We noticed that all mutants except the *arl-13* single mutant have a normal phenotype showing parallel elongation of PHA and PHB cilia. The PHA and PHB cilia

of a single *arl-13* mutant are misdirected, meaning they are not joined anywhere; they extend independently.

We questioned the hypothesis to understand better parallel cilia elongation: i) will ASE and ASE cilia also show similar misdirection phenotype in the absence of the ARL-13? ii) are the cilia length and phenotype independently controlled process? iii) can the basal body position affect cilia phenotype related to length? iv) how do different cilia-related essential genes affect the cilia direction?

The misdirection phenotype is seen in the ASE and ASI cilia without the ARL-13. We presented double mutants having different PHA lengths, and the misdirection of doubles does not have any significant difference from a single *arl-13* mutant. This data shows that the misdirection phenotype is independent of cilia length. We measured their distance to evaluate the basal body position and dendrite length for the next hypothesis. Briefly, the basal body position and dendrite length are not associated factors affecting cilia direction. Lastly, we generated various double and triple mutants to check their PHA and PHB cilia lengths and to understand interactions.

Interestingly, we found a severe phenotype in the *arl-13 (gk513); hdac-6 (ok3203); nphp-2 (gk653)* triple mutant, and therefore we can conclude that INV/NPHP-2 and HDAC6/HDAC-6 are involved in the regulation process of cilia with ARL13B/ARL-13. Another interesting result *is arl-13 (gk513); bbs-8 (nx77)* double mutant has a rescued phenotype. The misdirection phenotype is 58.80 % and 20.56 % in *arl-13 (gk513)* single and *arl-13 (gk513); bbs-8 (nx77)* double mutant, respectively. The misdirection phenotype is 38.26 % decreased in *arl-13 (gk513); bbs-8 (nx77)* double mutant. Therefore, we concluded that BBS-8 could partially rescue the misdirection phenotype.

4.2 Societal Impact and Contribution to Global Sustainability

Ciliopathy is a genetic condition originating from the organism's abnormal or dysfunctional cilia. This disease group is a member of the rare disease with its own disease-specific and exceptional clinical features. Joubert syndrome (JBTS) is one of the common genetic conditions, and forty-four different genes are associated with this disorder. The ARL13B/*arl-13* is a well-known gene of this disease with characteristic abnormal cilia structure, called misdirection in this thesis. Abnormal cilia structure directly affects cilia functionality. ASE and ASI cilia, for example, are located near the mouth of *C. elegans*, and they are responsible for taking food into the organism by sensing environmental signals. Chemical, mechanical and optical signals also taken by cilia. However, misdirected ASE and ASI cilia cause a change in the ciliary bundle in the mount. Therefore cilia can not extend to outside for sensing the environment. Similar to ASE and ASI cilia, PHA and PHB cilia misdirection also affects the sensation.

In this thesis, we aimed to understand how the cilia directions of ASE/ASI and PHA/PHB are regulated in *C. elegans* when specific proteins are absent. We analyzed various single, double and triple mutants by tagging them with different fluorescent proteins. Therefore, we tested the effects of different proteins involved in this regulation. We screened twenty-three different genes which are associated with cilia and cilia-related processes. Also, we made unique fluorescent transgenics to visualize ASE and ASI cilia. We analyzed different cilia types from the same perspective to support our aim. This study is significant because of the understanding of how the cilia direction is regulated. The knowledge about cilia direction can be a preliminary study for studying human cilia to understand ciliopathy diseases better. Based on the National Institutes of Health report, the prevalence of JBTS is a person of 80-90.000 worldwide. To decrease this number, it is essential to have a comprehensive understanding of cilia and cilia-related regulations. As a result, this thesis introduces a novel perspective to the research on cilia, and we present a significant result: the misdirection phenotype of ARL13B partially rescues via BBS8.

4.3 Future Prospects

In this thesis, we analyzed PHA and PHB cilia structure labelling with numerous fluorescent markers for classification as normal and misdirection cilia. As a further aspect of this study, high-resolution microscope techniques like electron microscope can be showed misdirection phenotype in ASE & ASI and PHA & PHB cilia. The interaction between misdirection and adhesion molecules also can be questioned. Adhesion molecules are proteins located at the cell/organelle surface for attachment to other structures [74]. The primary function of these molecules is to transfer cellular signals into the cell and adjacent cells. Flagellar adhesion molecules have been shown in unicellular organisms such as *Tetrahymena thermophila* [75], *Euplotes octocarinatus* [76], and *Chlamydomonas reinhardtii* [77], where they play a crucial role in mating. Specifically, agglutinins, a member of glycoproteins, are involved in the mating process in the green algae *Chlamydomonas* [77]. In addition to single-cellular organisms, marine larvae have ciliary adhesion molecules to encourage the capturing of particles while feeding [78]. Furthermore, glycoprotein molecules in the adhesion system stabilize cilia-cilia interaction [79]. Carolyn Ott and colleagues demonstrated that cilia communicate in rod photoreceptors and cholangiocytes by involving ciliary adhesion molecules. Together with this study, we can hypothesize that adhesion molecules can regulate cilia direction by interacting between cilia and ciliary membrane. Additional investigation may be carried out by explicitly focusing on glycoproteins in cilia and the ciliary membrane to better understand the mechanism responsible for cilia directionality.

One potential future outcome of this study is determining cilia-specific genes that only express a cilium in the cilia bundle. The *C. elegans* Neuronal Gene Expression Map & Network (CeNGEN) comprises gene expression profiles in the nematode *C. elegans* [80]. This system allows the determination of cilium-specific genes by choosing some parameters. Wild-type worms can be mutated to target a specific gene region using the CRISPR system to analyse the effect of specific genes in cilia. Then their cilia direction in the cilia bundle can be investigated. Furthermore, mammalian studies can be involved with the same perspective as *C. elegans*.

BIBLIOGRAPHY

[1] J. Pan, "Cilia and ciliopathies: From Chlamydomonas and beyond," *Sci. China C Life Sci.*, vol. 51, no. 6, pp. 479–486, Jun. 2008, doi: 10.1007/s11427-008-0071-3.

[2] F. K. Bangs, N. Schrode, A.-K. Hadjantonakis, and K. V. Anderson, "Lineage specificity of primary cilia in the mouse embryo," *Nat. Cell Biol.*, vol. 17, no. 2, pp. 113–122, Feb. 2015, doi: 10.1038/ncb3091.

[3] D. N. Wheatley, "Primary Cilia in Normal and Pathological Tissues," *Pathobiology*, vol. 63, no. 4, pp. 222–238, 1995, doi: 10.1159/000163955.

[4] C. J. Haycraft, B. Banizs, Y. Aydin-Son, Q. Zhang, E. J. Michaud, and B. K. Yoder, "Gli2 and Gli3 localize to cilia and require the intraflagellar transport protein polaris for processing and function," *PLoS Genet.*, vol. 1, no. 4, p. e53, Oct. 2005, doi: 10.1371/journal.pgen.0010053.

[5] D. Huangfu and K. V. Anderson, "Cilia and Hedgehog responsiveness in the mouse," *Proc. Natl. Acad. Sci.*, vol. 102, no. 32, pp. 11325–11330, Aug. 2005, doi: 10.1073/pnas.0505328102.

[6] K. C. Corbit, A. E. Shyer, W. E. Dowdle, J. Gaulden, V. Singla, and J. F. Reiter, "Kif3a constrains β-catenin-dependent Wnt signalling through dual ciliary and non-ciliary mechanisms," *Nat. Cell Biol.*, vol. 10, no. 1, pp. 70–76, Jan. 2008, doi: 10.1038/ncb1670.

[7] J. M. Gerdes *et al.*, "Disruption of the basal body compromises proteasomal function and perturbs intracellular Wnt response," *Nat. Genet.*, vol. 39, no. 11, pp. 1350–1360, Nov. 2007, doi: 10.1038/ng.2007.12.

[8] S. Habbig *et al.*, "NPHP4, a cilia-associated protein, negatively regulates the Hippo pathway," *J. Cell Biol.*, vol. 193, no. 4, pp. 633–642, May 2011, doi: 10.1083/jcb.201009069.

[9] E. J. Ezratty, N. Stokes, S. Chai, A. S. Shah, S. E. Williams, and E. Fuchs, "A Role for the Primary Cilium in Notch Signaling and Epidermal Differentiation during Skin Development," *Cell*, vol. 145, no. 7, pp. 1129–1141, Jun. 2011, doi: 10.1016/j.cell.2011.05.030.

[10] D. Meng and J. Pan, "Chlamydomonas: Cilia and Ciliopathies," in *Chlamydomonas: Biotechnology and Biomedicine*, M. Hippler, Ed., in Microbiology Monographs, vol. 31. Cham: Springer International Publishing, 2017, pp. 73–97. doi: 10.1007/978-3-319-66360-9_4.

[11] G. A. Greenan, R. D. Vale, and D. A. Agard, "Electron cryotomography of intact motile cilia defines the basal body to axoneme transition," *J. Cell Biol.*, vol. 219, no. 1, p. e201907060, Jan. 2020, doi: 10.1083/jcb.201907060.

[12] S. T. Christensen, L. B. Pedersen, L. Schneider, and P. Satir, "Sensory Cilia and Integration of Signal Transduction in Human Health and Disease," *Traffic*, vol. 8, no. 2, pp. 97–109, Feb. 2007, doi: 10.1111/j.1600-0854.2006.00516.x.

[13] R. S. Molday and O. L. Moritz, "Photoreceptors at a glance," *J. Cell Sci.*, vol. 128, no. 22, pp. 4039–4045, Nov. 2015, doi: 10.1242/jcs.175687.

[14] K. F. Atkinson *et al.*, "Dopaminergic signaling within the primary cilia in the renovascular system," *Front. Physiol.*, vol. 6, Apr. 2015, doi: 10.3389/fphys.2015.00103.

[15] N. F. Berbari, A. K. O'Connor, C. J. Haycraft, and B. K. Yoder, "The Primary Cilium as a Complex Signaling Center," *Curr. Biol.*, vol. 19, no. 13, pp. R526–R535, Jul. 2009, doi: 10.1016/j.cub.2009.05.025.
[16] P. M. Jenkins, D. P. McEwen, and J. R. Martens, "Olfactory Cilia: Linking Sensory Cilia Function and Human Disease," *Chem. Senses*, vol. 34, no. 5, pp. 451–464, Jun. 2009, doi: 10.1093/chemse/bjp020.
[17] N. Falk, M. Lösl, N. Schröder, and A. Gießl, "Specialized Cilia in Mammalian Sensory Systems," *Cells*, vol. 4, no. 3, pp. 500–519, Sep. 2015, doi: 10.3390/cells4030500.
[18] S. Wang, J. C. Burton, R. R. Behringer, and I. V. Larina, "In vivo micro-scale tomography of ciliary behavior in the mammalian oviduct," *Sci. Rep.*, vol. 5, no. 1, p. 13216, Aug. 2015, doi: 10.1038/srep13216.
[19] S. A. Halbert, P. Y. Tam, and R. J. Blandau, "Egg Transport in the Rabbit Oviduct: The Roles of Cilia and Muscle," *Science*, vol. 191, no. 4231, pp. 1052–1053, Mar. 1976, doi: 10.1126/science.1251215.
[20] T. B. Warrington, "Computational and molecular dissection of an X-box cis-Regulatory module," 2018, doi: 10.48550/ARXIV.1810.00478.
[21] J. Lee and Y. D. Chung, "Ciliary subcompartments: how are they established and what are their functions?," *BMB Rep.*, vol. 48, no. 7, pp. 380–387, Jul. 2015, doi: 10.5483/BMBRep.2015.48.7.084.
[22] S. Kim and B. D. Dynlacht, "Assembling a primary cilium," *Curr. Opin. Cell Biol.*, vol. 25, no. 4, pp. 506–511, Aug. 2013, doi: 10.1016/j.ceb.2013.04.011.
[23] T. Kobayashi and B. D. Dynlacht, "Regulating the transition from centriole to basal body," *J. Cell Biol.*, vol. 193, no. 3, pp. 435–444, May 2011, doi: 10.1083/jcb.201101005.
[24] J. F. Reiter and M. R. Leroux, "Genes and molecular pathways underpinning ciliopathies," *Nat. Rev. Mol. Cell Biol.*, vol. 18, no. 9, pp. 533–547, Sep. 2017, doi: 10.1038/nrm.2017.60.
[25] L. Wang *et al.*, "Ciliary transition zone proteins coordinate ciliary protein composition and ectosome shedding," *Nat. Commun.*, vol. 13, no. 1, p. 3997, Jul. 2022, doi: 10.1038/s41467-022-31751-0.
[26] D. A. Hoey, M. E. Downs, and C. R. Jacobs, "The mechanics of the primary cilium: An intricate structure with complex function," *J. Biomech.*, vol. 45, no. 1, pp. 17–26, Jan. 2012, doi: 10.1016/j.jbiomech.2011.08.008.
[27] S. Chaaban and G. J. Brouhard, "A microtubule bestiary: structural diversity in tubulin polymers," *Mol. Biol. Cell*, vol. 28, no. 22, pp. 2924–2931, Nov. 2017, doi: 10.1091/mbc.e16-05-0271.
[28] G. Garcia, D. R. Raleigh, and J. F. Reiter, "How the Ciliary Membrane Is Organized Inside-Out to Communicate Outside-In," *Curr. Biol.*, vol. 28, no. 8, pp. R421–R434, Apr. 2018, doi: 10.1016/j.cub.2018.03.010.
[29] K. I. Hilgendorf, C. T. Johnson, and P. K. Jackson, "The primary cilium as a cellular receiver: organizing ciliary GPCR signaling," *Curr. Opin. Cell Biol.*, vol. 39, pp. 84–92, Apr. 2016, doi: 10.1016/j.ceb.2016.02.008.
[30] K. G. Kozminski, K. A. Johnson, P. Forscher, and J. L. Rosenbaum, "A motility in the eukaryotic flagellum unrelated to flagellar beating.," *Proc. Natl. Acad. Sci.*, vol. 90, no. 12, pp. 5519–5523, Jun. 1993, doi: 10.1073/pnas.90.12.5519.
[31] Y. Cao, A. Park, and Z. Sun, "Intraflagellar Transport Proteins Are Essential for Cilia Formation and for Planar Cell Polarity," *J. Am. Soc. Nephrol.*, vol. 21, no. 8, pp. 1326–1333, Aug. 2010, doi: 10.1681/ASN.2009091001.

[32] D. G. Cole, D. R. Diener, A. L. Himelblau, P. L. Beech, J. C. Fuster, and J. L. Rosenbaum, "Chlamydomonas Kinesin-II–dependent Intraflagellar Transport (IFT): IFT Particles Contain Proteins Required for Ciliary Assembly in Caenorhabditis elegans Sensory Neurons," *J. Cell Biol.*, vol. 141, no. 4, pp. 993–1008, May 1998, doi: 10.1083/jcb.141.4.993.
[33] T. Kobayashi, Y. Ishida, T. Hirano, Y. Katoh, and K. Nakayama, "Cooperation of the IFT-A complex with the IFT-B complex is required for ciliary retrograde protein trafficking and GPCR import," *Mol. Biol. Cell*, vol. 32, no. 1, pp. 45–56, Jan. 2021, doi: 10.1091/mbc.E20-08-0556.
[34] S. K. Singh, M. Gui, F. Koh, M. C. Yip, and A. Brown, "Structure and activation mechanism of the BBSome membrane protein trafficking complex," *eLife*, vol. 9, p. e53322, Jan. 2020, doi: 10.7554/eLife.53322.
[35] S. Nozaki, R. F. Castro Araya, Y. Katoh, and K. Nakayama, "Requirement of IFT-B-BBSome complex interaction in export of GPR161 from cilia," *Biol. Open*, vol. 8, no. 9, Sep. 2019, doi: 10.1242/bio.043786.
[36] G. M. Liew *et al.*, "The Intraflagellar Transport Protein IFT27 Promotes BBSome Exit from Cilia through the GTPase ARL6/BBS3," *Dev. Cell*, vol. 31, no. 3, pp. 265–278, Nov. 2014, doi: 10.1016/j.devcel.2014.09.004.
[37] T. Eguether *et al.*, "IFT27 Links the BBSome to IFT for Maintenance of the Ciliary Signaling Compartment," *Dev. Cell*, vol. 31, no. 3, pp. 279–290, Nov. 2014, doi: 10.1016/j.devcel.2014.09.011.
[38] M. V. Nachury *et al.*, "A Core Complex of BBS Proteins Cooperates with the GTPase Rab8 to Promote Ciliary Membrane Biogenesis," *Cell*, vol. 129, no. 6, pp. 1201–1213, Jun. 2007, doi: 10.1016/j.cell.2007.03.053.
[39] J. L. Badano, N. Mitsuma, P. L. Beales, and N. Katsanis, "The Ciliopathies: An Emerging Class of Human Genetic Disorders," *Annu. Rev. Genomics Hum. Genet.*, vol. 7, no. 1, pp. 125–148, Sep. 2006, doi: 10.1146/annurev.genom.7.080505.115610.
[40] M. G. Turan, M. E. Orhan, S. Cevik, and O. I. Kaplan, "CiliaMiner: an integrated database for Ciliopathy Genes and Ciliopathies," Bioinformatics, preprint, Nov. 2022. doi: 10.1101/2022.11.28.518070.
[41] C. E. Larkins, G. D. G. Aviles, M. P. East, R. A. Kahn, and T. Caspary, "Arl13b regulates ciliogenesis and the dynamic localization of Shh signaling proteins," *Mol. Biol. Cell*, vol. 22, no. 23, pp. 4694–4703, Dec. 2011, doi: 10.1091/mbc.e10-12-0994.
[42] C. Casalou, A. Ferreira, and D. C. Barral, "The Role of ARF Family Proteins and Their Regulators and Effectors in Cancer Progression: A Therapeutic Perspective," *Front. Cell Dev. Biol.*, vol. 8, p. 217, Apr. 2020, doi: 10.3389/fcell.2020.00217.
[43] S. Cevik *et al.*, "Joubert syndrome Arl13b functions at ciliary membranes and stabilizes protein transport in Caenorhabditis elegans," *J. Cell Biol.*, vol. 188, no. 6, pp. 953–969, Mar. 2010, doi: 10.1083/jcb.200908133.
[44] T. Caspary, C. E. Larkins, and K. V. Anderson, "The Graded Response to Sonic Hedgehog Depends on Cilia Architecture," *Dev. Cell*, vol. 12, no. 5, pp. 767–778, May 2007, doi: 10.1016/j.devcel.2007.03.004.
[45] K. Bouhouche, P. Le Borgne, M. Lemullois, and A.-M. Tassin, "La paramécie, un organisme modèle pour étudier la ciliogenèse et les maladies ciliaires," *médecine/sciences*, vol. 37, no. 6–7, pp. 632–638, Jun. 2021, doi: 10.1051/medsci/2021087.
[46] J. M. Brown and G. B. Witman, "Cilia and Diseases," *BioScience*, vol. 64, no. 12, pp. 1126–1137, Dec. 2014, doi: 10.1093/biosci/biu174.
[47] V. Rajagopalan, E. O. Corpuz, M. J. Hubenschmidt, C. R. Townsend, D. J. Asai, and D. E. Wilkes, "Analysis of Properties of Cilia Using Tetrahymena thermophila," in

Cytoskeleton Methods and Protocols, R. H. Gavin, Ed., in Methods in Molecular Biology, vol. 586. Totowa, NJ: Humana Press, 2009, pp. 283–299. doi: 10.1007/978-1-60761-376-3_16.
[48] N. A. Zaghloul and N. Katsanis, "Zebrafish Assays of Ciliopathies," in *Methods in Cell Biology*, Elsevier, 2011, pp. 257–272. doi: 10.1016/B978-0-12-381320-6.00011-4.
[49] T. G. Fai, L. Mohapatra, P. Kar, J. Kondev, and A. Amir, "Length regulation of multiple flagella that self-assemble from a shared pool of components," *eLife*, vol. 8, p. e42599, Oct. 2019, doi: 10.7554/eLife.42599.
[50] J. L. Rosenbaum, J. E. Moulder, and D. L. Ringo, "FLAGELLAR ELONGATION AND SHORTENING IN CHLAMYDOMONAS," *J. Cell Biol.*, vol. 41, no. 2, pp. 600–619, May 1969, doi: 10.1083/jcb.41.2.600.
[51] E. N. Allen, J. Ren, Y. Zhang, and J. Alcedo, "Sensory systems: their impact on C. elegans survival," *Neuroscience*, vol. 296, pp. 15–25, Jun. 2015, doi: 10.1016/j.neuroscience.2014.06.054.
[52] D. B. Doroquez, C. Berciu, J. R. Anderson, P. Sengupta, and D. Nicastro, "A high-resolution morphological and ultrastructural map of anterior sensory cilia and glia in Caenorhabditis elegans," *eLife*, vol. 3, p. e01948, Mar. 2014, doi: 10.7554/eLife.01948.
[53] S. Britz *et al.*, "Structural Analysis of the Caenorhabditis elegans Dauer Larval Anterior Sensilla by Focused Ion Beam-Scanning Electron Microscopy," *Front. Neuroanat.*, vol. 15, p. 732520, Nov. 2021, doi: 10.3389/fnana.2021.732520.
[54] Z. F. Altun and D. H. Hall, "WormAtlas Hermaphrodite Handbook - Nervous System - Neuronal Support Cells," *WormAtlas*, Apr. 2003, doi: 10.3908/wormatlas.1.19.
[55] S. Brenner, "THE GENETICS OF *CAENORHABDITIS ELEGANS*," *Genetics*, vol. 77, no. 1, pp. 71–94, May 1974, doi: 10.1093/genetics/77.1.71.
[56] H. Wickham, *ggplot2: Elegant Graphics for Data Analysis*. New York, NY: Springer New York, 2009. doi: 10.1007/978-0-387-98141-3.
[57] A. Kassambara, *rstatix: Pipe-Friendly Framework for Basic Statistical Tests*. 2023. [Online]. Available: https://CRAN.R-project.org/package=rstatix
[58] *R a language and environment for statistical computing: reference index*. Vienna: R Foundation for Statistical Computing, 2010.
[59] J. Mijalkovic, J. van Krugten, F. Oswald, S. Acar, and E. J. G. Peterman, "Single-Molecule Turnarounds of Intraflagellar Transport at the C. elegans Ciliary Tip," *Cell Rep.*, vol. 25, no. 7, pp. 1701-1707.e2, Nov. 2018, doi: 10.1016/j.celrep.2018.10.050.
[60] J. van Krugten, N. Danné, and E. J. G. Peterman, "TRPV channel OCR-2 is distributed along *C. elegans* chemosensory cilia by diffusion in a local interplay with intraflagellar transport," Biophysics, preprint, Nov. 2020. doi: 10.1101/2020.11.19.390005.
[61] J. M. Brown, D. A. Cochran, B. Craige, T. Kubo, and G. B. Witman, "Assembly of IFT Trains at the Ciliary Base Depends on IFT74," *Curr. Biol.*, vol. 25, no. 12, pp. 1583–1593, Jun. 2015, doi: 10.1016/j.cub.2015.04.060.
[62] O. İs. Kaplan, "*RPI-1* (human *DCDC2*) displays functional redundancy with Nephronophthisis 4 in regulating cilia biogenesis in *C. elegans*," *Turk. J. Biol.*, vol. 47, no. 1, pp. 74–83, Jan. 2023, doi: 10.55730/1300-0152.2642.
[63] P. Canning *et al.*, "CDKL Family Kinases Have Evolved Distinct Structural Features and Ciliary Function," *Cell Rep.*, vol. 22, no. 4, pp. 885–894, Jan. 2018, doi: 10.1016/j.celrep.2017.12.083.
[64] M. S. Pir *et al.*, "CilioGenics: an integrated method and database for predicting novel ciliary genes," Bioinformatics, preprint, Apr. 2023. doi: 10.1101/2023.03.31.535034.

[65] M. He, S. Agbu, and K. V. Anderson, "Microtubule Motors Drive Hedgehog Signaling in Primary Cilia," *Trends Cell Biol.*, vol. 27, no. 2, pp. 110–125, Feb. 2017, doi: 10.1016/j.tcb.2016.09.010.
[66] R. O'Hagan *et al.*, "Glutamylation Regulates Transport, Specializes Function, and Sculpts the Structure of Cilia," *Curr. Biol.*, vol. 27, no. 22, pp. 3430-3441.e6, Nov. 2017, doi: 10.1016/j.cub.2017.09.066.
[67] C. Schouteden, D. Serwas, M. Palfy, and A. Dammermann, "The ciliary transition zone functions in cell adhesion but is dispensable for axoneme assembly in C. elegans," *J. Cell Biol.*, vol. 210, no. 1, pp. 35–44, Jul. 2015, doi: 10.1083/jcb.201501013.
[68] P. Shi *et al.*, "HDAC6 Signaling at Primary Cilia Promotes Proliferation and Restricts Differentiation of Glioma Cells," *Cancers*, vol. 13, no. 7, p. 1644, Apr. 2021, doi: 10.3390/cancers13071644.
[69] Halloran, D. Fitzpatrick, and A. M. Burnell, "The chemosensory system of Caenorhabditis elegans and other nematodes," pp. 71–88, Jan. 2006.
[70] S. R. F. Warburton-Pitt, M. Silva, K. C. Q. Nguyen, D. H. Hall, and M. M. Barr, "The nphp-2 and arl-13 Genetic Modules Interact to Regulate Ciliogenesis and Ciliary Microtubule Patterning in C. elegans," *PLoS Genet.*, vol. 10, no. 12, p. e1004866, Dec. 2014, doi: 10.1371/journal.pgen.1004866.
[71] O. E. Blacque, "Loss of C. elegans BBS-7 and BBS-8 protein function results in cilia defects and compromised intraflagellar transport," *Genes Dev.*, vol. 18, no. 13, pp. 1630–1642, Jul. 2004, doi: 10.1101/gad.1194004.
[72] X. Pan *et al.*, "Mechanism of transport of IFT particles in C. elegans cilia by the concerted action of kinesin-II and OSM-3 motors," *J. Cell Biol.*, vol. 174, no. 7, pp. 1035–1045, Sep. 2006, doi: 10.1083/jcb.200606003.
[73] M. Brunnbauer *et al.*, "Regulation of a heterodimeric kinesin-2 through an unprocessive motor domain that is turned processive by its partner," *Proc. Natl. Acad. Sci.*, vol. 107, no. 23, pp. 10460–10465, Jun. 2010, doi: 10.1073/pnas.1005177107.
[74] D. B. Abrams *et al.*, "Adhesion Molecules," in *Encyclopedia of Behavioral Medicine*, M. D. Gellman and J. R. Turner, Eds., New York, NY: Springer New York, 2013, pp. 39–40. doi: 10.1007/978-1-4419-1005-9_1254.
[75] J. Wolfe, S. Mpoke, and S. F. Tirone, "Cilia, Ciliary Concanavalin A-Binding Proteins, and Mating Recognition in Tetrahymena thermophila," *Exp. Cell Res.*, vol. 209, no. 2, pp. 342–349, Dec. 1993, doi: 10.1006/excr.1993.1319.
[76] E. Plümper, M. Freiburg, and K. Heckmann, "Conjugation in the Ciliate Euplotes octocarinatus: Comparison of Ciliary and Cell Body-Associated Glycoconjugates of Non-mating-Competent, Mating-Competent, and Conjugating Cells," *Exp. Cell Res.*, vol. 217, no. 2, pp. 490–496, Apr. 1995, doi: 10.1006/excr.1995.1114.
[77] R. Kooijman *et al.*, "Wheat germ agglutinin induces mating reactions in Chlamydomonas eugametos by cross-linking agglutinin-associated glycoproteins in the flagellar membrane.," *J. Cell Biol.*, vol. 109, no. 4, pp. 1677–1687, Oct. 1989, doi: 10.1083/jcb.109.4.1677.
[78] M. R. Romero, H. C. P. Kelstrup, and R. R. Strathmann, "Capture of Particles by Direct Interception by Cilia During Feeding of a Gastropod Veliger," *Biol. Bull.*, vol. 218, no. 2, pp. 145–159, Apr. 2010, doi: 10.1086/BBLv218n2p145.
[79] C. Ott, N. Elia, S. Y. Jeong, C. Insinna, P. Sengupta, and J. Lippincott-Schwartz, "Primary cilia utilize glycoprotein-dependent adhesion mechanisms to stabilize long-lasting cilia-cilia contacts," *Cilia*, vol. 1, no. 1, p. 3, Dec. 2012, doi: 10.1186/2046-2530-1-3.
[80] S. R. Taylor *et al.*, "Molecular topography of an entire nervous system," *Cell*, vol. 184, no. 16, pp. 4329-4347.e23, Aug. 2021, doi: 10.1016/j.cell.2021.06.023.

[81] J. Schindelin *et al.*, “Fiji: an open-source platform for biological-image analysis,” *Nat. Methods*, vol. 9, no. 7, pp. 676–682, Jul. 2012, doi: 10.1038/nmeth.2019.

Appendix

An exhaustive list of the materials and equipment used to prepare the strains and perform the analysiss

Microscope, Software and Algorithms	**Supplier**	**Model or Order Number**
Andor iQ 3.6.2 software	ANDOR	
Andor iXon ultra EMCCD	ANDOR	253.3.5/16/14996
Carl Zeiss microscope	CARL ZEISS	Axio Vert.A1
Compound microscope	LEICA	LEICA DM6 B
Fluorescence stereo microscope	LEICA	LEICA M205 FA
Stereo microscopes	LEICA	LEICA S9I
ZEISS LSM 900 with Airyscan 2	ZEISS	
ZEISS ZEN 3.0 (Blue edition)	ZEISS	
ImageJ	Schindelin et al., 2012 [81]	https://imagej.nih.gov/ij/download.html - Version 1.53o
R Core Team (Version 4.1.2)	N/A	https://www.r-project.org/
Equipments	**Supplier**	**Model or Order Number**
Molecular Imager Gel Doc XR+ System with Image Lab Software	Bio-Rad	1708195
Autoclave (steam sterilizer)	Tuttnauer	3850ELC-D
	Nüve steam Art	OT 90L
Centrifuge	Thermo Scientific™	MicroCL 21R Microcentrifuge
	Thermo Scientific™	MicroCL 21 Microcentrifuge
Cooled incubator	Panasonic	MIR-554-PA
Cover glass	ISOLAB	075.00.004
Cryogen tube (2 mL)	Biosigma	CL2ARBEPSTS
Electronic balance	Precisa	LS 1200C SCS
	SHIMADZU	ATX 224
Electrophoresis	Thermo Scientific™	Owl EasyCast™ B2
	Thermo Scientific™	Owl EasyCast™ B1
Halocarbon oil	Sigma-ALDRICH	H8898 - 50 mL
Heater	NARISHIGE	PC-100
Ice system	Scotsman	AF 80 AS 230/50/1
Immersion oil	Sigma-ALDRICH	56822 - 50 mL
Individual (PCR) tubes (0.2 mL)	Thermo Scientific	AB-0620
Injection neddle	WPI	TW100F-4

Laminar flow hood	Nucleon Laboratory Instruments	Class II Biosafety cabinet
Magnetic stirrers	Heidolph	MR HEI-TEC
Micro centrifuges	GYROZEN	KGZS23518120872
Microscope slide	ISOLAB	I.075.05.003
Microwave oven	Vestel	MD 20 MB
Multi-channel pipettes (1-10 µl)	Thermo Scientific	OH22524
Oil Hydraulic Micromanipulator	NARISHIGE	MMO-4
Parafilm	Bemis	PM-996
PCR thermal cyclers	Thermo Fisher Scientific	ProFlex PCR System
	Bio-Rad	C1000 Touch Thermal Cycler
Petri dishes 60 x 15 mm 90 x 15 mm	FIRATMED	 8870000046 8870000011
Pipette tips 10 µl 200 µl	ISOLAB	 005.01.001 005.01.002
Pipette tips 1000 µl	Biosigma	 17A0845
Pipettes 0.2-2 µl 1-10 µl 2-20 µl 10-100 µl 20-200 µl 100-1000 µl	Thermo Scientific	PH77343 NH30094 PH79581 JH97441 JH95162 JH95573
Pressure supply port	NARISHIGE	IM-400
Pure nitrogen tank	Gazsan	GA-K2099096
S1 pipet filler	Thermo Scientific	187550
Serological pipettes 10 mL 25 mL	Biosigma Biosigma	 N403346 N403347
Spectrophotometer	Thermo Scientific™	NanoDrop™ 2000
Sterile filter unit with MF-Millipore (0.22 µm)	Millex® Syringe Filters	SLGS033SS
Sterile syringe (0.5 mL)	AYSET Tıbbi Ürünler	KD8354-00-10/17
Sterile syringe (10 mL)	Helmed	20160802
Ultra-Low Temperature (UTL) freezer	Haier	DW-86L62B
Vortex mixer	Stuart Biocote	SA8
Water purification system	Merck	ZRQSVP800
Waterbath	Thermo Scientific™	Precision™GP 02
	Thermo Scientific™	Precision™ GP 10
Weighing boats 30 mL 100 mL	ISOLAB	 WBPSN7030001 WBPSN7100001
Chemicals and Recombinant Proteins	**Supplier**	**Model or Order Number**
100bp Plus II DNA ladder	TRANSBIO	BM321-01
10X Easy Taq buffer	TRANSBIO	N21106
6X Loading buffer	TRANSBIO	GH101-01
Agar-Agar, Kobe I	CARL ROTH	5210.2 - 1 kg
Agarose	Prona Agarose Biomax	D00216PR
Bacto™ Peptone	BD Bioscience™	211677 - 500 gr
$CaCl_2$	CARLO ERBA REAGENTS	10043-52-4
Cholesterin	CARL ROTH	8866.1 - 100 gr
Easy Taq DNA polymerase	TRANSBIO	AP111-01
EDTA	CARLO ERBA REAGENTS	6381-92-6
Ethanol	ALKOKİM	01012018-IR.01
Ethidium bromide	BioShop	ETB444.1

Glacial acetic acid	ISOLAB	64-19-7
High Pure dNTPs	TRANSBIO	AD101-02
K_2HPO_4	Merck	105101.1000 - 1 kg
KCl	Merck	7447-40-7
KH_2PO_4	Merck	104873.1000 - 1 kg
LB Broth, Miller Formulation	VWR Life Science	J106 - 1 kg
$MgCl_2$	Merck	7786-30-3
$MgSO_4.7H_2O$	CARLO ERBA REAGENTS	10034-99-8
Nystatin	RPI (Research Products International)	N82020-10.0
Primers	MACROGEN	
Proteinase K	Sigma-ALDRICH	SLBQ1035V
Sodium chloride (NaCl)	ISOLAB	969.033.1000 - 1 kg
Tris base	Sigma-ALDRICH	T1503 - 1 kg
Ultra pure water	Tekkim Kimya	TK.911010.0

Curriculum Vitae

June 2023

MERVE GUL TURAN

Bioengineering, Faculty of Life Science
Abdullah Gul University
Sumer Campus, Kayseri, Turkey

Lab site: Kaplan Lab
ORCID iD: 0000-0001-5783-7168

TRAINING & EDUCATION

2020 - Present

MSc., Bioengineering, Abdullah Gul University, Turkey
Thesis Title: "The characterisation of the cilia candidate gene(s)"
Advisor: Dr. Sebiha Cevik Kaplan

2017

Erasmus, Biotechnology, Polytechnic Institute of Coimbra, Portugal

2016 - 2021

BSc., Department of Mathematics, Halic University, Turkey
(Second Major Degree)

2015 - 2019

BSc., Department of Molecular Biology and Genetics, Halic University, Turkey

SCHOLARSHIP

2022 - 2023

Project: TUBITAK 1002 Project (12 Months)
Project Title: "The Characterization of Genes Related with Bardet-Biedl Syndrome in Ciliary Gate"
Funding Institution: TUBITAK
Project Coordinator: Dr. Sebiha Cevik Kaplan

2022 - 2023

Project: TÜSEB (8 Months)

Project No: 2022-ACİL-10

Project Title: "ARL13B-dependent joint elongation of two distinct cilia in Caenorhabditis elegans"

Funding Institution: TÜSEB

Project Coordinator: Dr. Sebiha Cevik Kaplan

PUBLICATIONS:

2022 - Turan, M. G., Kantarci, H., Temtek, S. D., Cakici, O., Cevik, S., & Kaplan, O. I. (2022). Protocol for determining the average speed and frequency of kinesin and dynein-driven intraflagellar transport (IFT) in *C. elegans*. **STAR Protocols**, 3(3), 101498. https://doi.org/10.1016/j.xpro.2022.101498

PREPRINT:

2022 - Turan, M. G., Orhan, M. E., Cevik, S., & Kaplan, O. I. (2022). CiliaMiner: an integrated database for Ciliopathy Genes and Ciliopathies. https://doi.org/10.1101/2022.11.28.518070 **bioRxiv (Submitted to Database)**

WEBSITE:

CiliaMiner - https://kaplanlab.shinyapps.io/ciliaminer/

WET LAB SKILLS:

- PCR and lysis
- Agarose gel electrophoresis
- Genetic cross
- Designing primer and sgRNA sets for CRISPR system
- Designing PCR primers

ANALYSIS:

- Using and analyzing analysis on a compound microscope
- Using and analyzing on a fluorescence microscope
- Drawing plots using a programming language (R)
- Figure preparation

CODE ABILITY

Good knowledge of R - https://github.com/mervegulturan

ABSTRACT PRESENTATIONS IN SCIENTIFIC MEETINGS

2022 8th International Congress of the Molecular Biology Association of Turkey
"Investigation of molecular mechanisms for the simultaneous elongation of two cilia"

2021 The 23rd International *C. elegans* Conference, Online
"Molecular Mechanism of Coordinating Cilia Intersection and Elongation"

2020 The 9th Internatıonal Molecular Biology And Bıotechnology Congress, Turkey
"Characterization of the voltage-gated K^+ channel gene, a novel cilia gene, in cilia biogenesis"